LUNDS UNIVERSITET

LTH

LUNDS TEKNISKA HÖGSKOLA

High Powered GASMAS Lung Diagnostics - Towards Larger Geometries

Detectability and Heating Limitations

Henrik Palme

Thesis for the degree of master of science in engineering

Supervisor: Anna-Lena Sahlberg

Project duration: 8 months

High Powered GASMAS Lung Diagnostics - Towards Larger Geometries

Detectability and Heating Limitations

by Henrik Palme

LUND
UNIVERSITY

Thesis for the degree of master of science in Engineering
Supervisor: Anna-Lena Sahlberg
Examiner: Joakim Bood

Frontpage by Henrik Palme.
A signal obtained during the project made into a pattern in the colors of the graphic profile of Lund University.

Typeset in LaTeX

Faculty of Engineering, Lund university
Department of Physics, Division of Combustion Physics

Abstract

The optical technique, *Gas in scattering media absorption spectroscopy* (GASMAS) shows promise in application to address current challenges in lung monitoring during intensive care, improving respiratory care by allowing for continuous, non-invasive monitoring. While the technique is already developed in neonatal infant care, the patient profile can be expanded by using higher powered laser systems, by increasing the geometries probed.

GASMAS is an optical technique that utilizes the scattering properties of gas-filled porous materials. In lung diagnostics, the lung tissue is probed, assessing the oxygen concentration present in the lungs. Since the light quickly attenuates by the tissue, a stronger light source is required to acquire a signal through larger patients.

To investigate the potential of expanding the geometries, this thesis assesses signal detectability when bulk absorbing material is added to the porous medium. Using a pork encased extruded polystyrene foam model and ex vivo porcine lungs, investigating SNR reduction and the oxygen absorption signal when pork-padding is added.

For high powered illumination, skin heating resulting in tissue damage to the patient was identified as a central risk. To assess this potential obstacle, the heating for different volunteers was assessed using two different illumination methods, free beam and probe illumination, different powers of the laser, along with skin tone and illumination area.

The results showed promise in future clinical applications demonstrating a strong SNR through thick pieces of pork padding both for the extruded polystyrene foam model and for the ex vivo porcine lungs. In heating, the area, illumination method, skin tone and illumination power all showed impacts on the resulting heating, exhibiting predictable patterns that can be used to assess heating risks in future clinical applications.

Both studies indicated a potential for future clinical applications, as well as a need for future research before the method can be implemented.

Populärvetenskaplig sammanfattning

Under Covid-19 pandemin, blev hela värden allvarligt påminda om hur livsviktiga våra lungor är. Under intensivvård övervakas lungorna noga för att snabbt och effektivt kunna åtgärda problem som kan uppstå. De nuvarande metoderna för att diagnostisera kollapsade lungor inkluderar röntgenstrålning. En effektiv metod, men som har några stora nackdelar. Röntgen ger bara en momentan bild av lungtillståndet, men kan inte kontinuerligt övervaka. En potentiell lösning till dessa utmaningar är att använda optiska metoder, som kan kontinuerligt övervaka lungornas funktioner och snabbt meddela sjukhuspersonal när tillståndet försämras.

Den optiska metoden som föreslås kallas GASMAS som står för *Gas in scattering media absorption spectroscopy*. Simplifierat kan man förklara GASMAS som att belysa huden med laserljus som sprids omkring i lungorna. Syrgas som finns i lungorna absorberar en del av ljuset vid rätt våglängd, vilket gör att man enkelt kan se när syrgaskoncentrationen i lungan reduceras.

Den här tekniken har redan utvecklats för användning på för tidigt födda spädbarn, som allt för ofta besväras av olika lungproblem. Företaget Neola Medical använder en jämförelsevis svag laser för att kontinuerligt övervaka lungaktiviteten hos barnen för att se till att problem snabbt kan åtgärdas. Men det är inte bara för tidigt födda spädbarn som kan få problem med lungorna. Så den här uppsatsen fokuserar på om den här metoden kan utvecklas för att utvidga patientgruppen till användning på större bebisar, barn och vuxna.

För att utforska dessa möjligheter används olika typer av modeller som ska efterlikna lungor. De första testerna görs på fläskinlindad frigolit, som påvisar många liknande egenskaper som lungvävnad. Tester på grislungor har också utförts, och olika tjocklek av fläsk har använts för att efterlikna mänsklig vävnad.

När en laser med högre effekt används uppkommer även ett helt annat problem, hur huden värms av laserljuset. Två olika belysningsmetoder undersöktes, både en laserstråle och en optisk prob som används i utvecklade kliniska metoder. Laserns effekt, storleken på ytan som belystes, och hudton utforskades som potentiella bidragande faktorer till hur huden värms av laserljuset.

Slutsatsen av uppsatsen var att de här teknikerna är värdefulla att fortsätta utforskas. En stark signal kunde ses genom grislungorna, även med tjocka bitar fläsk i vägen. Värmestudien påvisade ett linjärt samband mellan ljusets effekt och uppvärmningen samt ett linjärt samband mellan hudton och uppvärmning. Vidare kunde en tydlig skillnad observeras på uppvärmning beroende på belysningsmetod, då proben hindrade huden från att kylas av luften.

Acknowledgements

I would like to extend my sincerest gratitude to my supervisor Anna-Lena Sahlberg. I could not have asked for a better mentor. Your dedication to research and teaching not only produces great results, but also inspires the people around you. You have not only taught me the subject at hand, but shown me the entirety of what research can be, and inspired me when motivation were low.

I also want to thank the entire research team, Emelie Krite Svanberg, Katarina Svanberg, Sune Svanberg, Yeyue Lin and Sara Bergsten. Your expertise and experience has been invaluable to me during this project. During all parts of this project, your kindness and patience have enabled me to confidently explore this topic, and I have learned a lot from all of you. Thank you!

I want to thank the folks over at Neola Medical, for their guidance, participation and their generosity in letting me use their equipment, even though I destroyed some of it. A special thanks to Sara Bergsten and Rasmus Grönlund.

I want to thank my friends, Love Kildetoft, Isa Hendriks, Klara Lozani Gerdhem, Lovisa Nilsson and Sara Bengtsdotter for your company in the office and interesting conversation, weather it was research related or something entirely different. A special thanks to Love and Emma Axebrink for helping me with the structure and Latex. I also wanna thank my friends Kevin Schomper, Olle Gustavsson, Isak Korpskog and Finn Wiestål who have kept me company through the internet during late nights working on my thesis.

I also want to thank everyone who volunteered to be measured on, it is greatly appreciated.

I want to thank the division, with Joakim Bood in the lead for welcoming me, for taking the time to be interested in this research and for all of the Thursday fikas.

Finally I want to thank my family for their support during this journey, and to my baby nieces, Eira and Helle for inspiring me to keep on going.

Contents

List of Figures

List of Tables

Chapter 1

Introduction

1.1 Background

During the Covid-19 pandemic, the world was gravely reminded of the importance of respiratory care. Possible respiratory complications during intensive care are numerous, with different treatment plans. Complications include atelectasis and pneumothorax. Atelectasis is the collapse of a lung or part of a lung due to a loss of air in the alveoli while pneumothorax is a collection of air between the lung and the chest cavity, leading to the collapse of the lung or part of the lung. Both atelectasis and pneumothorax can be life threatening if not caught early. Common diagnostic tools for both pneumothorax and atelectasis include X-rays or CT-scans.[1][2] While effective, these methods only give a momentary view of the lung conditions, while also being highly ionizing and requiring expertise and resources. A continuous method of monitoring lung function could help patients and clinicians by alerting when function is compromised, enabling a fast therapeutic response. In this thesis, an optical technique by the name of GASMAS is proposed as a solution to this problem.

Gas in scattering media absorption spectroscopy (GASMAS) is an optical method based on *Tunable Diode Laser Absorption Spectroscopy* (TDLAS) that allows for gas concentration analysis in porous media. The material probed can range from pharmaceutical tablets and timber, to medical applications such as sinus and lung diagnostics. The method relies on the scattering of the material to enhance the effective path-length of the light increasing the absorption signal. This method has been utilized in the creation of two companies, GASPOROX AB [1] developing diagnostic methods for packaging logistics, and Neola Medical[2] who develops lung monitoring systems for neonatal infants. The small geometries of the neonatal infants enables the laser system to obtain diagnostic values using a relatively low power diode laser[3].

There have been numerous studies showing the potential in using GASMAS for lung diagnostics. Krite Svanberg et al. (2016)[4] showed promise in the technique by measurements of both oxygen gas concentrations and water vapour concentrations in the lungs of 29 healthy newborns, achieving an signal-to-noise ratio above 3. Krite Svanberg et al. (2021) [5] showed, in a proof of concept study that respiratory complications, such as pneumothorax and atelectasis can be identified in the GASMAS signal in sedated piglets [5].

The quick attenuation of the light when penetrating tissue becomes an obstacle when performing GASMAS lung diagnostics of patients larger than a neonatal infant. To allow for diagnostics on bigger patients, the laser power will therefore have to be increased. This was shown to have potential, being investigated

[1]GASPOROX AB (PUBL), Lund Sweden, info@gasporox.se,`https://gasporox.se/`

[2]Neola Medical AB, Lund Sweden, info@neolamedical.com,`https://www.neolamedical.com/`

by Lin et al. (2021)[6] by utilizing a pulsed laser to preform time-resolved spectroscopy to probe thick samples. The article also suggest the possibility of using an optically amplified CW system with a diffuser probe for internal illumination. Therefore, this thesis will investigate the possibilities of using a higher powered laser to expand the patient groups. A stronger laser contributes with other challenges as well, particularly how the tissue is heated as more light is illuminating the skin, risking damage to the patient. The aims and questions are therefore as follows.

- How does larger geometries and laser power impact the obtained signal for lung diagnostics using GASMAS?
- How does laser power, illumination area, skin tone and illumination method impact the skin heating?

This thesis is a continuation of the work preformed during three previous master theses, Anna Brandt (2022)[7], Emma Hjörneby (2022)[8] and Martin Molin (2020)[9]. A summary of these theses can be found in chapter 2.7.

1.2 Work Overview

This thesis is divided into two parts, *GASMAS Signal Evaluations - Model and Porcine Lung Measurements* evaluating the signal quality and detection limit and *Evaluating Skin Heat Development During Laser Illumination* evaluating heating by the laser.

For the signal evaluations, extruded polystyrene foam encased in pork and ex vivo porcine lungs were utilized to gain insight into the potential limitations of the method. The absorption and signal-to-noise ratio were evaluated for different signal types and thickness of pork padding in both cases.

For the heat evaluations two different illumination methods were utilized, a free beam with a circular cross section, 1 cm in diameter, and a fibre coupled probe from Neola Medical allowing for direct contact with the skin during light illumination. Different laser powers were investigated, along with area of illumination and the skin tone of volunteers.

Chapter 2

Theory

To fully understand the spectroscopic methods that are utilized in this thesis the interaction between light and matter, specifically the interaction with biological tissue needs to be evaluated. It is expected that the reader has a basic understanding of photonics and biology. The theory will focus on the specifics of light interaction with biological tissue.

2.1 Light-Matter Interaction

There are two main interactions that light has with any material, scattering and absorption. The internal mechanics of these interactions are quite complicated and will not be discussed in detail in this thesis. For further theory, the book *Atomic and Molecular Spectroscopy* by Sune Svanberg [10] is recommended.

2.1.1 Scattering

When an incident electromagnetic wave interacts with a particle. There is a probability of the process known as scattering to occur. Scattering can be seen as a change in direction for an incoming photon, deviating from its original direction into a new one. [11](p.125) If every direction of scattering would be equally probable, this process would be isotropic. This is however seldom the case, resulting in anisotropy. The direction of the scattering is described by the scattering phase function over a sphere, showing the probability of scattering. To describe this property, the anisotropy factor g is introduced. An anisotropy factor of 0 indicates equal probability of scattering in all possible directions (isotropic), a factor of 1 denotes only forward scattering (the photon continues in the same direction) and -1 denotes only backward scattering (the photon is reflected back towards its source). For biological tissue, the anisotropic factor lies between 0.8 and 0.98 which is highly forward scattering, most scattering occurs within 30°of the optical axis[11] (pp. 212-213). While this may allude to the light having a straight path trough the tissue, the amount of scattering events makes the light quickly lose its original direction. A figure showing the anisotropy of scattering is shown in Fig 2.1. While the scattering phase function is here shown as an ellipse, the function can come in many different shapes.

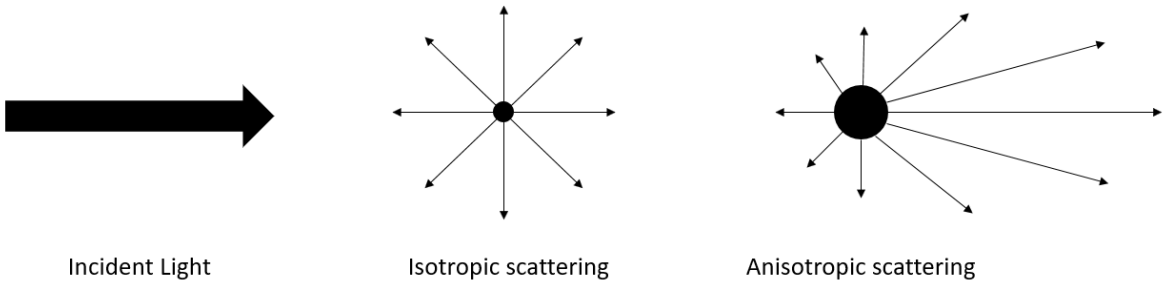

Figure 2.1: The process of isotropic and anisotropic light scattering. The incident light coming from the left, the smaller particle shows isotropic scattering (middle) while the larger particle shows anisotropic scattering (right). The length of the arrow indicates a proportionality to the scattering phase function.

There are two main models for scattering, Rayleigh- and Mie-scattering. Mie-scattering occurs when the particle that scatters the light is considerably bigger than the wavelength of the incident light while Rayleigh scattering occurs when the particle size is comparable to or smaller than the wavelength. Mie- and Rayleigh-scattering have different scattering probability density functions. Both the medium, size, shape, and the wavelength of the incident light impacts the scattering probability density function.[10](pp.65-66)[11](p.212)

While these models are both accurate and practical in interactions with well defined particles, biological tissue is complex, with structures of both varying size and shape, making modelling difficult. The anisotropic factor of biological tissue along with approximations of the scattering coefficients are utilized as a substitute of these precise models.

2.1.2 Absorption

When incident light interacts with an atom or molecule, and the right conditions are met, there is a probability that the particle absorbs the photon, resulting in an excitation to a higher energy state.[11](p.122) For singular atoms, excitation means electrons being lifted from a lower energy state to a higher energy state. Molecules, however, have more ways to store energy, electronic, vibrations and rotations. Electronic transitions requiring the most energy, followed by vibrations, and rotation being the least energetic. [10](pp.55-60)

The energy levels for both atoms and molecules are discrete, with different rates of vibration and rotation along with electronic levels. All processes can be involved during an excitation. Since the excited levels are discrete, only photons of a certain frequency can be absorbed by the molecule, this is known as on resonance[10](p.52). For molecules in gas form, such as oxygen gas, the absorption spectrum exhibits sharp peaks where photons can be absorbed. [12] Figure 2.2 shows the absorption spectrum for selected wavelength for oxygen gas. While gas typically has very sharp absorption peaks, matter in liquid or solid form has a more continuous spectrum, exhibiting slowly varying absorption and scattering coefficients over the frequency spectrum. [12]

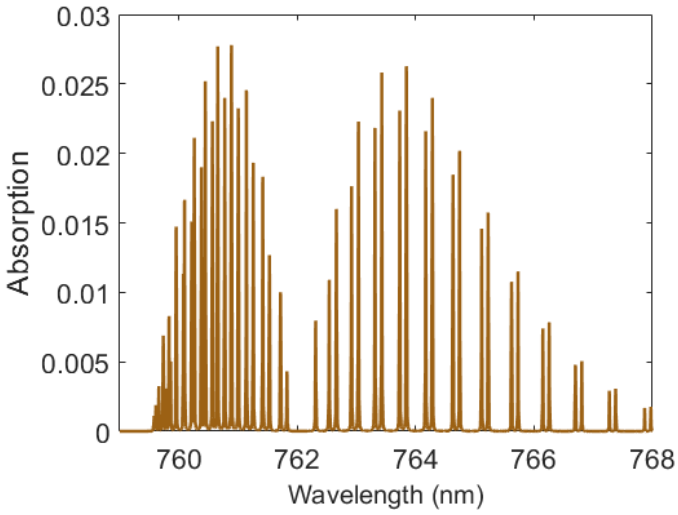

Figure 2.2: The absorption spectrum for 21% oxygen gas with 100 cm in path length over a selection of wavelengths.

2.1.3 Line Shapes

While the peaks in the absorption spectrum for oxygen gas may seem infinitely thin, as observed in Figure 2.3, there is some broadness that makes transitions possible even when the incident photons are not exactly the right frequency. This feature is called line broadening and arises for many different reasons that are briefly described below. [13](pp. 71-74)

- **Lifetime broadening:** Also called natural broadening, is a consequence of the Heisenberg uncertainty principle. Both the lifetime of the excited state and the energy cannot be determined without uncertainty. This leads to an uncertainty of the transition energy, and thereby the frequency of the photon, resulting in line broadening. This broadening effect is always present but is often overshadowed due to its weak nature.
- **Doppler broadening:** The particles that interact with the light have a velocity as a consequence of the heat present in the material. This velocity results in a shift in the perceived frequency of the incident light due to relativity, the Doppler effect. Particles moving away from the light source will experience a lower frequency and vice versa, resulting in a broadening of the absorption peak. This process is dependent on the temperature of the material, which can be utilized in thermometry.
- **Pressure broadening:** Particle collisions in the gas results in perturbation of the particle, by shifting the energy levels or by altering the lifetime of the state, resulting in an uncertainty in the transition energy, and thereby a broadening of the frequency. This process is dependent on the pressure of the sample.

These mechanisms are mostly important for spectroscopy in gases where the atoms/molecules are free. For solid and liquid material the density is much higher resulting in peaks that are numerous and broadened exhibiting a continuous spectrum. The shape of the broadening also differs between the broadening mechanisms. For most gas applications the life-time broadening is overshadowed by the Doppler and pressure broadening. The shape of the Doppler broadening is Gaussian while the shape for pressure broadening is Lorentzian. The combination of these two is called the Voigt profile and is shown in Figure 2.3.[13](pp. 71-74)

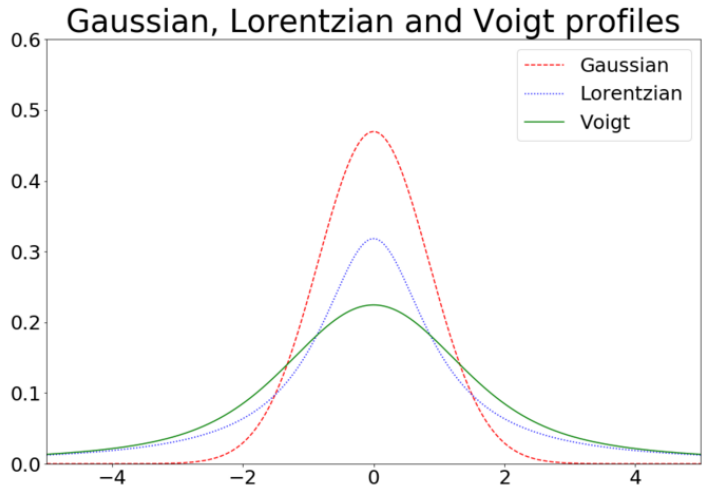

Figure 2.3: The shape of a Gaussian, Lorentzian and a Voigt profile.[14]

2.1.4 Beer-Lambert Law

The Beer-Lambert law describes the decrease in intensity of incident light due to absorption and scattering when penetrating a medium. The absorption coefficient μ describes the likelihood of absorption occurring, and is dependent on the medium and wavelength. A gaseous medium can be assumed to be non-scattering, as the scattering is much less than the absorption and is slowly varying with wavelength, while the absorption is strongly frequency dependent. The absorption coefficient will therefore be used in the formula. With the path-length of L and incident intensity of I_0 results in an intensity of I. [11](pp. 127-128)

$$I = I_0 e^{-\mu L} \tag{2.1}$$

This version of the Beer-Lambert law is highly idealized, and applications in highly scattering media, determining the path-length may be an obstacle. A way to circumvent this problem will be presented further along.

2.2 Tunable Diode-Laser Absorption Spectroscopy (TDLAS)

One of the simplest methods in gas spectroscopy is tunable diode-laser absorption spectroscopy. The method utilizes the sharp absorption peaks of gasses to assess the concentration of a gas within a system. An absorption peak of the gas is selected to use for the analysis, the frequency of the light is then scanned across the absorption peak. Assuming a system without any noticeable scattering, and if the absorption coefficient is known, the concentration of the gas can be easily evaluated by using the Beer-Lambert law. The path-length of the light is known, and the intensity before and after interaction is recorded over the sweep. The tunable diode-lasers that are utilized are easily scanned across a selected absorption peak. Fine tuning of the light emitted is obtained by scanning the driving current, resulting in a scan of the output power as well. Typically, a linear triangular ramping of the wavelength and thereby the power output is utilized. Scanning over the absorption peak then results in a decrease of signal in the ramping form of the output light. The depth of this decrease can then be evaluated to assess the concentration using a linear regression on the remaining recorded spectrum. Since the output power over time scales with frequency, the generated time spectrum can be calibrated to instead show frequency. An example of how a recorded spectrum

can look as well as a schematic picture of a simplified setup is shown in Figure 2.4. This method requires ideal conditions, without noticeable scattering and a known optical path.[15]

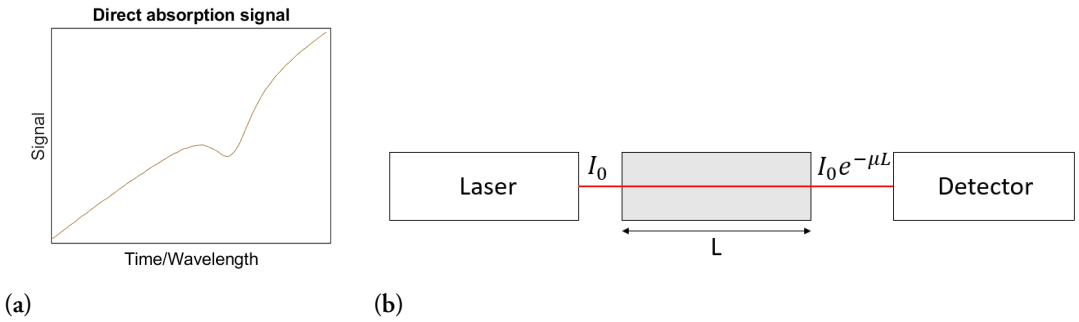

(a) (b)

Figure 2.4: A typical signal from TDLAS (a) along with a schematic picture showing a simplified setup (b).

2.3 Gas in Scattering Media Absorption Spectroscopy (GASMAS)

A fundamental issue with spectroscopic methods in biological tissue is the turbidity of the medium. When light enters the tissue it is scattered rapidly, loosing its original direction. The high absorption of the tissue is also a challenge, inhibiting light from penetrating the sample. GASMAS is a subset of absorption spectroscopy where the turbidity of the media is instead utilized. The basis for this method is investigating a material with pores, gas filled holes within the medium. Light scatters around in the tissue where it might cross a pore, if the light is of the right frequency there is a probability of absorption by the gas, which results in a intensity decrease, similarly to TDLAS. The scattering enables the light to travel effectively much longer than the distance between source and detector which makes the signal of the absorption spectroscopy much larger.[12] The detected light is however much smaller due to absorption and scattering by the tissue. The fraction of detected light is also dependent on the geometries measured. Larger geometries require longer path lengths for the light, increasing the likelihood of absorption by the bulk medium, requiring higher laser power to attain a detectable signal.[6] The detection of gas stems from the surrounding solid and liquid bulk material having absorption and scattering coefficients that vary little over the utilized frequencies, while the gas has a dramatic increase in absorption for the selected absorption peak. This phenomenon is shown in figure 2.5, demonstrating the resulting intensity decrease on the slightly varying bulk material absorption and scattering.[12] A challenging aspect of the method is that while the effective path-length is elongated due to the scattering, it is unknown. In TDLAS the path-length is a known parameter, resulting in the concentration of the studied sample as the only variable. This issue can be mitigated by using two light sources, one that measures the target gas, and another one that measures a gas with a known concentration to determine the effective path-length.[3]

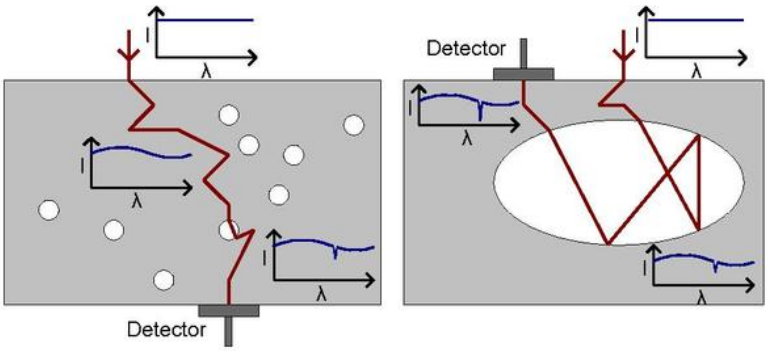

Figure 2.5: A schematic figure showing the light trajectories in small pore GASMAS (left) and large pore GASMAS (right).[16]

2.4 GASMAS Lung Monitoring

Since lung tissue is a porous material, exhibiting gas filled pores called alveoli, GASMAS can be used to assess the gas concentrations within these pores. This technique is utilized by the company Neola Medical. Their system utilizes the GASMAS technique for continuous lung monitoring of neonatal infants. It is not uncommon for neonatal infants to suffer from defective lungs, either pneumothorax (lung collapse) or other decreases in lung function including respiratory distress syndrome and atelectasis. Current methods for monitoring are either non-continuous (X-ray and ultrasound) or visual monitoring. These methods suffer from different drawbacks, X-ray and ultrasound being non-continuous and visual monitoring suffering from the human factor and resource inefficiency. GASMAS measurements have the benefit of being both continuous and objective. The power of the laser is very low, but still penetrates through the lungs due to the small geometries that are measured. The system uses two frequencies, one that is tuned for the oxygen gas absorption peak and one that is tuned for water vapour. The laser that is tuned to water vapour is used to assess the effective path-length. The concentration of water vapour can easily be determined using temperature and pressure of the lung, allowing the effective path-length to be assessed via the GASMAS measurements. This circumvents the issue of unknown effective path-length that was formulated in the GASMAS section. A fibre-coupled emitter probe is placed on the chest while the detector is placed in the armpit. The emitter probe allows for a flat emission profile of the light in to the body. The main parameter of interest is how the signal changes over time, a sudden change indicating a pneumothorax while a prolonged gradual decrease in signal indicates a gradual decrease in lung function. [3]

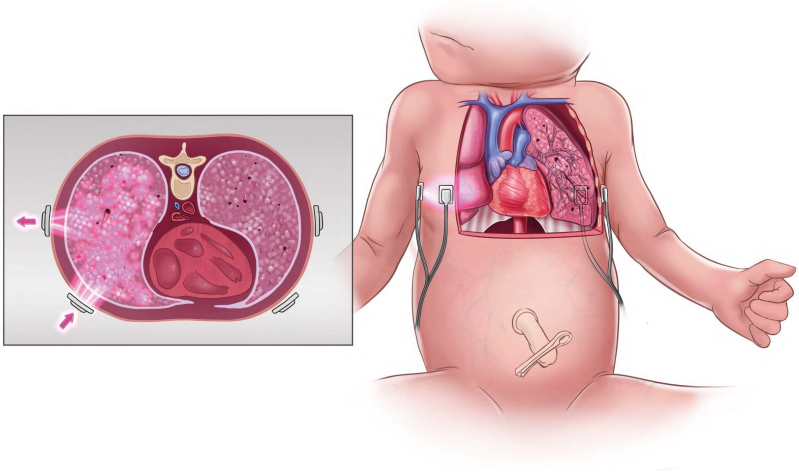

Figure 2.6: An illustration showing the light-path and placement of emitter probe and detector for GASMAS measurements on an infant. Published by Neola Medical AB, used with permission.[3]

2.5 Light Interaction with Tissue

While spectroscopy in gasses can be simple, issues arise when the light needs to penetrate tissue. Our bodies are complex systems with numerous different molecules and structures. Light that enter the body is quickly attenuated which inhibits the ability to obtain a signal through tissue. To mitigate this issue, the wavelength range of the incident light may be chosen to reduce the absorption of light by the tissue, allowing for light transmission through larger geometries of biological tissue. The major components of tissue, such as liquid water, fat etc. has a reduced absorption coefficient in the interval of around 600 to 1150 nm which is in the red and near infrared region of the electromagnetic spectrum. This interval is often called the therapeutic optical window, since it is ideal for clinical applications. Figure 2.7 shows the major components of tissue along with the absorption coefficient. [11](p.130-131)

The frequencies that are used for GASMAS measurements, utilized by Neola medical are absorption peaks for oxygen gas and water vapour that lie within the therapeutic optical window, allowing for light penetration through biological tissue.[3]

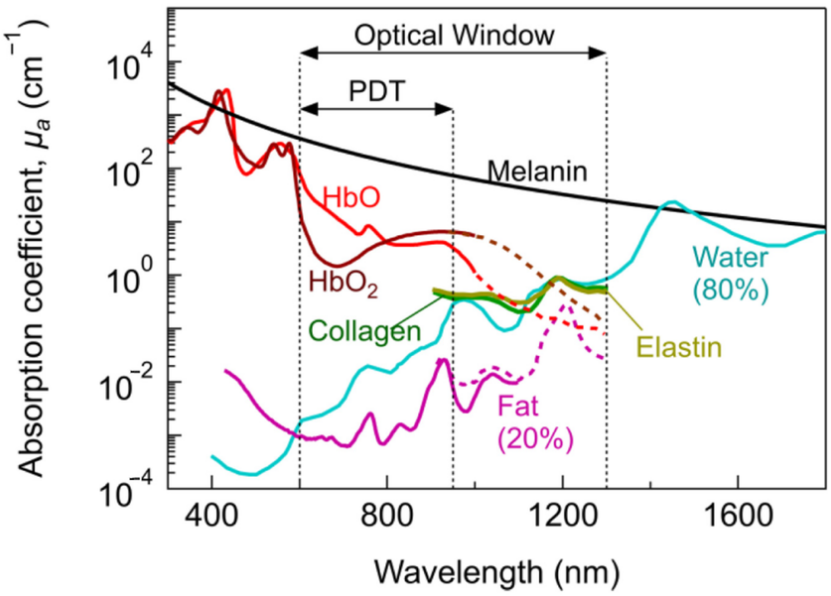

Figure 2.7: The absorption coefficient for some common molecules in human tissue demonstrating the therapeutic optical window, as published by Algorri et al.[17]

2.6 Tissue Thermodynamics

When light is absorbed by tissue, heat often develops through internal conversions in the molecules [18](p.23). For clinical application this method may result in risk of tissue damage, if the heat developed is too big. While GASMAS lung diagnostics on neonatal infants uses a low power of the laser avoiding this issue, when investigating the possibility of using a higher power, this risk must be taken into account. It is well known, that most of the light is absorbed in the top layers of the skin. The skin is therefore the point of interest for potential tissue damage from heating. To understand the potential damage to the skin by laser illumination, cooling and heating of the skin has to be evaluated.[19]

There are three ways of cooling in thermodynamics, Planck radiation, heat conduction and convection, biological tissue exhibiting a fourth mechanism, heat transport by blood flow.

- **Planck radiation:** All bodies with a temperature emit radiation, called Planck radiation or black body radiation. The emitted spectrum is broad and is characterized by the emissivity, the effectiveness of emitting thermal radiation, where a value of 1 denotes a theoretical black body. Not only does this process slightly cool the surface, but it can also be utilized to assess temperatures using infrared cameras.
- **Conduction:** When a thermal equilibrium is not present in a body, heat will travel through the material to cooler areas, effectively spreading out the thermal energy over the material.
- **Convection:** The surrounding air is cooler than the skin, heating the air which is then replaced by new cool air. The skin is typically around 30 °C while the surrounding air is typically around 20 °C. This process may be mitigated by covering the area, either inhibiting air to get in direct contact with the skin, or by trapping the heated air.
- **Blood flow:** The above mentioned cooling mechanics assumes a stationary body, however, there is fluid flowing inside the body in the form of blood. The heat will therefore also be transported away by the blood stream.

2.7 Previous Research

As mentioned in the introduction, there have been three previous masters theses conducted on this subject, Anna Brandt (2022)[7], Emma Hjörneby (2022)[8] and Martin Molin (2020)[9].

The addition of a new laser system using a tapered amplifier has enabled this thesis to expand the scope of these previous theses, allowing for a higher illumination power while exhibiting the modulation properties that are required for GASMAS measurements, and allowing for higher powered illumination in heat evaluation.

2.7.1 Gas in scattering media absorption spectroscopy in Large Geometries - Anna Brandt (2022)

This thesis focused on ways to increase the geometries for GASMAS measurements. Utilizing a low powered 760 nm diode laser on extruded polystyrene foam and wild boar lung. The opportunity to incorporate an optical tapered amplifier (OPTA) into the system to enhance the power was also investigated. Finally a 2 W continuous-wave 760 nm laser was used to investigate how light can penetrate different thickness of pork. However, this system could not be used to detect gas, due to limits in wavelength tuning.[7]

The low powered tunable CW system could produce a GASMAS signal through 3-5 cm of tissue with about 25 mW in power. The incorporation of the OPTA into the optical system may have amplified the light slightly but was hindered due to the sensitivity of the coupling. Finally a good signal was obtained from a 1 W system through 14 cm of tissue.[7]

2.7.2 Simulations and modeling of light propagation in biological tissue - Emma Hjörneby (2022)

In this thesis Monte Carlo simulations, using the tool *Multi-Scattering*[1], were performed on scattered light in biological tissue. GASMAS measurements with a diode laser were performed on wild boar lung. A Titanium-sapphire laser with a max output of 2W was used to see transmission through different thickness of pork gammon, and transmission signal-to-noise ratio evaluated to determine potential for future measurements in larger tissue phantoms. [8]

The simulations showed promise in understanding the lights trajectory and the fraction of light that is transmitted. Since the other experiments are shared with the previous thesis, the conclusions are similar. [8]

2.7.3 In-vivo assessment of unwanted tissue heating during near infrared laser light emission - Martin Molin (2020)

In this thesis both simulations and experiments were carried out to determine heating in skin when illuminating with laser light. A relevant model was created for the equilibrium position for heat development in tissue. Monte Carlo simulations were performed to determine the scattering of the photons and Finite Element Method (FEM) was used to model heat development. Measurements of temperature during illumination was done on 12 volunteers using both the arm and the lower inner lip as a replacement for internal tissue. Different powers, wavelengths and areas were evaluated. [9]

[1] `https://multi-scattering.com/`

Conclusions include that the heating is linearly dependent on the laser power. It is recommended to use a larger area to avoid tissue heating. The simulations, while not entirely representing the reality are a valuable tool to evaluate how heat might develop for new applications. [9]

Chapter 3

Instrumentation

This chapter describes the laser system and other instrumentation used in the GASMAS measurements and heating evaluation.

3.1 The Laser System

It is clear for GASMAS, a light-source that has a tunable wavelength is needed. The wavelength needed for GASMAS in tissue with oxygen as its targeted gas needs to to be tunable at a specific wavelength allowing absorption by oxygen while within the therapeutic optical window. A diode laser is suitable due to its ability to be tuned at a high modulation frequency. It exhibits, however, a low power and needs to be enhanced for this application. A tapered amplifier is a device that enhances the power emitted by the laser diode and will be used to circumvent this obstacle. The tapered amplifier can be seen as a pn-junction with a current enhancing the power of the laser light. The theory of tapered amplifiers will not be discussed further in this thesis and can be read about in "Narrow-linewidth master-oscillator power amplifier based on a semiconductor tapered amplifier" by Wilson et al. [20]. The specific laser system that is used in this project is a tapered amplified diode laser from Toptica Photonics (TA Pro 765)[1]. The system has the ability to be frequency modulated over a range of frequency of around $\pm$ 12 GHz, and the sweep frequency is set to 25 Hz. The central frequency of the light is tunable and is for the application selected to 392.5 THz/763.8 nm which corresponds to the targeted absorption line for the oxygen gas. The output power of the system is adjustable partially via the control-box (Toptica DLC pro)[2]. Since the laser light is aligned into an optical fibre via a fibre-coupler, precise tuning of the output power from the optical fibre can be achieved by adjustment of the fibre-coupler.

3.2 GASMAS Signal Evaluations - Models and Porcine Lung Measurement

Below, the different parts of the optical setup will be described. A diagram showing the connections between the components is shown in Figure 3.2.

[1] https://www.toptica.com/products/tunable-diode-lasers/amplified-lasers/ta-pro

[2] https://www.toptica.com/products/tunable-diode-lasers/laser-driving-electronics/dlc-pro

Detector

For the detectability assessment measurement, a Photodiode Hamamatsu S3590-08 detector[3] with an area of 10x10 mm was used. In front of the detector an interference filter (Thorlabs FBH 760-10[4]) was placed, with the purpose to negate the effect of other light sources in the room (ceiling lights, light from equipment etc.). This helps reduce the noise in the signal and allows for a higher amplification of the signal to ensure that the signal accurately corresponds to the incoming light from the laser. The filter can be seen as a band-pass filter, only transmitting light with a frequency within the allowed window.

Amplifier

For the signal to be visible on the oscilloscope the detector is connected to an amplifier (DHPCA-100 Variable Gain 200 MHz wideband current amplifier[5]). To ensure proper signal quality, the amplifier was always turned to the highest setting allowed before overloading the amplifier. The signal shown on the oscilloscope can therefore not always be compared between measurements due to different levels of amplification.

Oscilloscope

To display the signal and obtain data, an oscilloscope (LeCroy HDO6104A[6]) was used. While the unprocessed signal from the amplifier may seem noisy, the oscilloscope has the ability to both smooth the signal by using a moving average function over the unprocessed signal, and to average the signal over time, improving the signal-to-noise ratio. In the results, both the unprocessed and the processed signals will be evaluated.

Diffusion Probe

For internal illuminations of the porcine lungs, it was necessary to diffuse the light emitted from the optical fibre, to avoid potential heating damage to the lung. A temporary probe was therefore built by inserting the optical fibre into Teflon piping that is commonly used for gas lines. The end of the laser fibre was placed approximately 3 cm from the end of the tube and the hole was plugged with extruded polystyrene foam balls. Teflon was chosen due to it being a highly scattering and heat resistant material and therefore able to diffuse the light without melting from the heat. The emission from the probe was ensured to be sufficient with the power meter. Figure 3.1 shows a picture of the probe taken during emission, along with a schematic picture or its components. A professional diffusers, while ideal, was not available during this work.

[3] https://www.hamamatsu.com/eu/en/product/optical-sensors/photodiodes/si-photodiodes/S3590-08.html

[4] https://www.thorlabs.com/thorproduct.cfm?partnumber=FBH760-10

[5] https://www.femto.de/en/products/current-amplifiers/variable-gain-up-to-200-mhz-dhpca.html

[6] https://www.testwall.com/product/teledyne-lecroy-hdo6104a-ms/

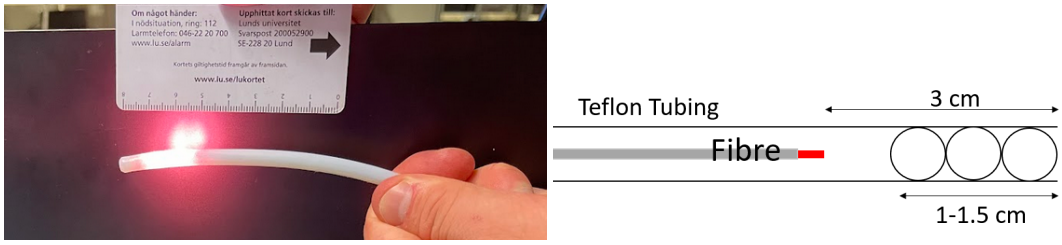

(a) (b)

Figure 3.1: The created emitter probe using Teflon tubing, extruded polystyrene foam and the laser fibre. A picture of the created emitter probe (a) and a schematic picture showing the probes components (b).

Nitrogen/Argon Gas

During the measurements it was important to determine if the GASMAS signal that was obtained was actually from the measured specimen and not from any other oxygen absorption along the light path. When the laser is emitting light, the DLC pro control box has a built-in power meter showing the output power over the sweeps at the exit of the TA pro laser system. This graph shows a decrease in output where the absorption line for the oxygen is located in the sweep. This is due to the light path inside the laser box reducing the light intensity by being absorbed by the oxygen in the air. Since the objective is to only measure the gas present in the sample, the absorption along the light path in the laser system needs to be removed. To accomplish this, a steady flow of nitrogen or argon gas (depending on availability) was pumped into the laser box. This was shown to be effective since the absorption caused by the air in the laser box disappeared after flushing. The flow was initially set high to fill the box, and then decreased to $\sim$ 0.3 l/min gas flow to maintain the gas in the box.

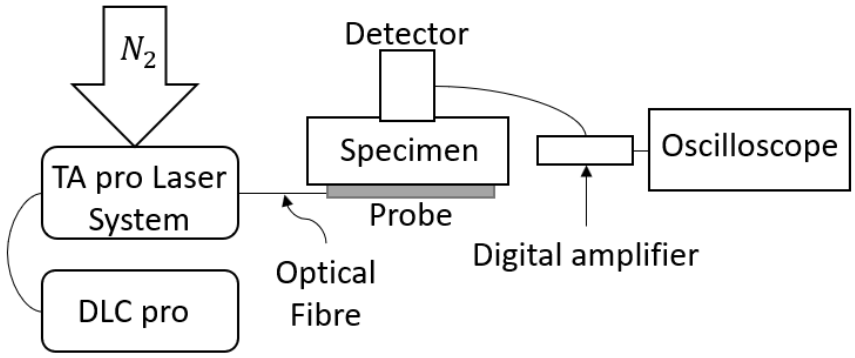

Figure 3.2: A schematic picture showing the setup for an arbitrary measurement.

3.3 Evaluating Skin Heat Development During Laser Illumination

3.3.1 Free Beam Measurements

A schematic picture of the setup can be found in figure 3.4. The optical fibre was mounted on a fiber holder. Due to the large divergence angle of the light, it was essential to place a positive lens with a short focal length after the fibre. For further collimation of the beam, another positive lens was placed in the beam path. The goal of the optical setup was not to gain a perfectly collimated beam but rather having a

beam with a sufficiently long beam waist to mitigate any modulation in the illumination area during the measurements. After the second lens an aperture was placed. This aperture was used to ensure correct illumination area and to cut out any side lobes that exhibited lower intensity than the center of the beam. After the aperture, a foldable power meter is mounted, assuring the right intensity of the beam. Finally a holder was made to place the arm for measurements. The holder had the simple function of ensuring that the arm did not move significantly during the measurements. The holder was also mounted with a target that ensured that the right size was obtained with the aperture. To collect the measurements a thermal camera was used (Flir C5[7]). The thermal camera has the ability to measure the highest temperature within a selected area along with the temperature of a small indicator allowing for quick measurements of the illuminated area and reference area.

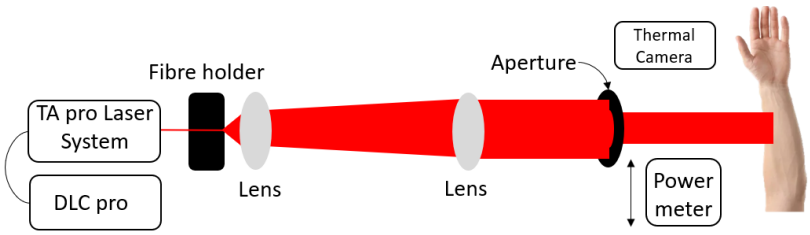

Figure 3.3: A schematic picture showing the optical setup of the free beam temperature measurements.

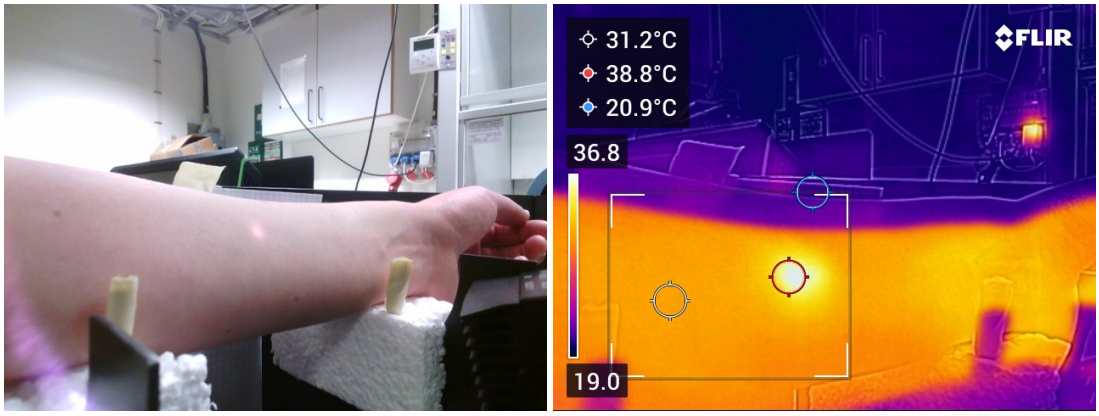

(a) (b)

Figure 3.4: A picture of the arm being measured on during a free beam measurement (a), the temperatures obtained during the same measurement (b). Note hat the red circle is located at the illuminated point automatically measuring the highest temperature point within the black box. The white circle is manually placed to measure the reference temperature.

3.3.2 Probe Measurements

A schematic picture of the setup can be found in Figure 3.5. For the probe measurements the setup was less complicated. The emitter probe provided by Neola Medical AB was used. The probe consist of an optical fibre and a 44 mm^2 optical diffuser that distributes the light evenly over this area. The probe was placed in front of the power meter and tuned to the correct power. The probe was then placed on the skin. Under the probe, a thermistor was placed, taped to the skin to ensure proper measurements. A reference was obtained by taping a thermistor to the skin, away from the area that was illuminated.

[7] `https://www.flir.eu/products/c5/`

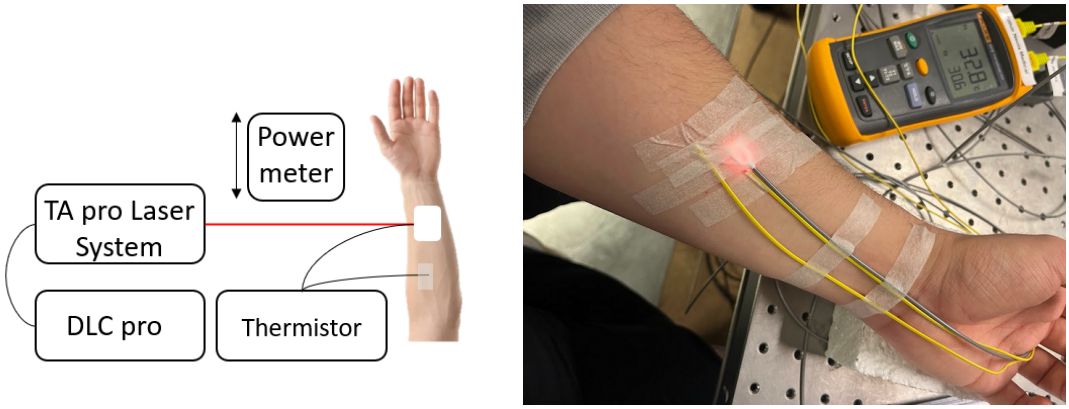

(a) (b)

Figure 3.5: A schematic picture showing the optical setup of the probe temperature measurements (left) and a picture from the measurements (right).

Chapter 4

GASMAS Signal Evaluations - Model and Porcine Lung Measurements

A central question in regards to GASMAS measurements is the ability to reliably obtain an oxygen GASMAS signal through tissue. The legibility of the signal can easily be found by obtaining the signal-to-noise ratio or SNR. A high SNR indicates that the decrease in signal due to the absorption of the light by oxygen in the sample is easily observed and analyzed, while a low SNR denotes that the signal is highly covered by noise. How much the absorbing material can be increased while still having a legible signal is central in evaluating diagnostics through bigger geometries. If a reliable relationship between SNR and absorption padding can be established, limits to the method in terms of SNR can be determined.

To determine if there is viability in GASMAS measurements for lung diagnostics in larger geometries, it has to be evaluated how the GASMAS signal from oxygen absorption is affected by the addition of absorption padding. When adding absorbing material, the effective path-length trough the gaseous pores in the medium should not be effected, resulting in a constant absorption signal. This will therefore be evaluated for different models and specimen evaluating the possible change of the ideally constant signal.

4.1 GASMAS Absorption in Extruded Polystyrene Foam and Porcine Lung Models

4.1.1 Pork Encased Extruded Polystyrene Foam

Extruded polystyrene foam (commonly known as Styrofoam) is a useful material to use for GASMAS measurements since it is highly scattering and exhibits a very low absorption. It is also a porous material resulting in a strong GASMAS signal. While extruded polystyrene foam is not the best model for lung tissue on its own, it was utilized to ensure the setup was working correctly.

A simple model that is used in this work to mimic the properties of human lung tissue is a thin extruded polystyrene foam block between two or more pieces of pork. The pork acts as both a scatterer and as an absorber of the light while not exhibiting gaseous pores that might result in a GASMAS signal. The extruded polystyrene foam included acts as the porous material exhibiting a GASMAS absorption signal. This was used to show how the quality of the signal deteriorates when a heavily absorbing material is impacting the signal.

Measurements were performed on two thicknesses of extruded polystyrene foam, 2.5 cm and 5 cm. Pork pieces, 2 cm in thickness was utilized as padding. The first measurement was on the block without padding, a piece of pork was then placed in front of the detector for the second set of measurement, another piece was added in front of the emitter probe, then another one in front of the detector, finally a fourth piece was placed in front of the detector for a total of 4 pieces with a total thickness of 8 cm. To ensure a maximum power of the probe being emitted into the model, aluminum foil was placed under the probe. Figure 4.1 shows a schematic picture and a picture of the set-up.

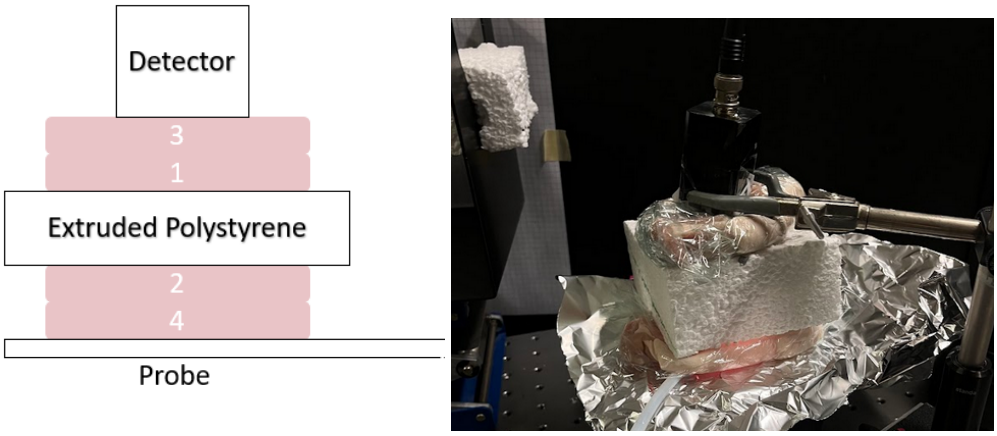

(a) (b)

Figure 4.1: The setup used for the extruded polystyrene foam measurements. The pork in the schematic picture are numbered in the order they were added to the setup.

Results

For the absorption assessment results, different parameters will be considered to gain a full understanding of the signal quality, both before and after data processing. While data processing will be presented step by step in Appendix A.2, examples will be shown in this chapter.

Figure 4.2 shows two different GASMAS signals that have been obtained during the pork encased extruded polystyrene foam measurements. The sweep of interest has been isolated to show the GASMAS signal more clearly. The figures shows the signal obtained from measurements performed on the 2.5 cm (left) and 5 cm (right) thick extruded polystyrene foam block without pork padding. Absorption is obtained by dividing the strength of the signal at the lowest point of the GASMAS signal with the corresponding value of the linear regression at the same time value. This fraction is then subtracted from one to obtain the fraction of light lost due to absorption by the oxygen gas. It is clear that the 5 cm thick extruded polystyrene foam block exhibits a stronger GASMAS signal, which will be apparent when discussing the results later in this chapter.

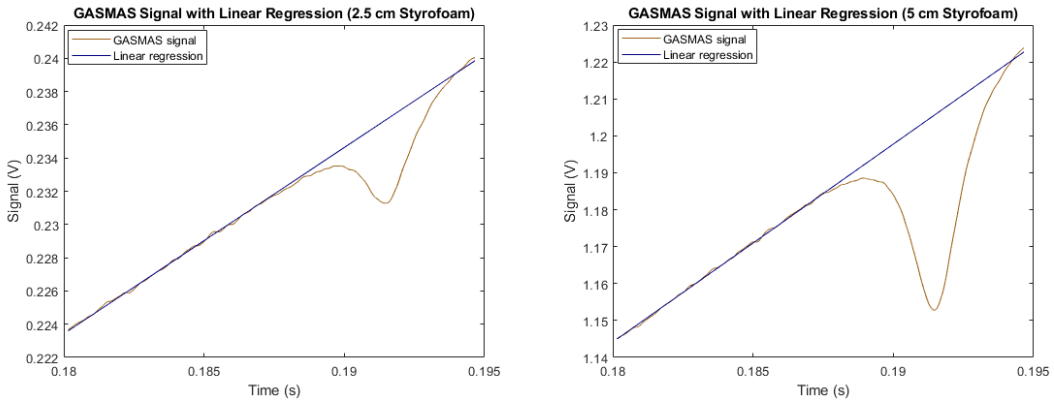

(a) (b)

Figure 4.2: The GASMAS signals obtained from measurements performed on 2.5 cm (a) and 5 cm (b) thick extruded polystyrene foam blocks without pork padding, along with linear regressions.

Table 4.1 shows the obtained GASMAS absorption signal from the pork encased extruded polystyrene foam calculated in accordance with Appendix A.2. The different thickness of both extruded polystyrene foam and pork padding are shown along with the obtained values. The mean value for the 2.5 cm thick extruded polystyrene foam was 2.2% and for the 5 cm thick extruded polystyrene foam was 4.5%, excluding the last value.

Table 4.1: The absorption in percent for the measurements for the signals in relation to the linear fit.

Extruded polystyrene foam thickness (cm)	Pork thickness (cm)	Absorption (%)
2.5	0	2.13
2.5	2	2.30
2.5	4	2.15
2.5	6	2.17
2.5	8	2.09
5	0	4.39
5	2	4.87
5	4	4.78
5	6	4.09
5	8	2.56

4.1.2 Porcine Lung Measurements

During two different days measurements on ex-vivo porcine lung were carried out. They were performed within 24 hours of slaughter and were purchased from a nearby slaughterhouse. The lungs differed in weight and volume as well as overall organ quality. During the first series of measurements one pair of lungs were used, and the following week three pairs were used. Below a step by step process of preparing the lungs will be presented.

- **Intubating and inflating the lung pair:** To ensure that the selected gas could fill the lung pair, the lung pair was intubated using a 7 mm endotracheal tube. Depending on lung quality and which measurement was done, either one of the lungs or both lungs were being ventilated. The endotracheal tube is connected to a bag, which in turn is connected to a steady flow of gas. The lung is ventilated by pressing down the bag, pushing the gas into the lung. The different gasses that were used for the measurements are: air, pure oxygen and pure nitrogen. While the intubation with bag

ventilation was preferred, for leaking lungs that were difficult to maintain inflated, a tube with constantly flowing gas was inserted directly into the lung as an alternative. Two pictures, showing both bag intubation and flowing gas intubation can be seen in Figure 4.3.

- **Hydration:** While measurements were carried out, the lungs were continuously drying out. To mitigate this process the lungs were being sprayed with water when necessary.
- **Collecting the data:** For each measurement the lung was either filled with oxygen or nitrogen gas. In some cases two measurement of each gas was recorded. The different signals obtained will be addressed in a later portion.

(a) (b)

Figure 4.3: Measurements being performed on a lung being ventilated with a bag (a) and with a tube directly inserted into the lung (b).

There are two main types of illumination methods that were utilized on the porcine lungs, external and internal.

- **External:** For external measurements the laser was administered on the outside of the lung using the diffuser probe, and the detector was placed on the other side of the lung lobe. Pieces of pork were placed either between the probe and the lung or between the detector and the lung. The lung was then filled with gas and measurements were carried out.
- **Internal:** For internal measurements the laser was instead administered on the inside of the lung by using the diffuser probe while the detector was placed on the outside of the lung lobe. Pieces of pork were placed between the detector and the lung. The lung was then filled with gas an measurements were carried out.

The reason for using these two methods is to investigate possible clinical applications. The external method is what is currently being utilized by Neola Medical, the method is therefore investigated to possibly expand the patient profile. While the external method is ideal in a clinical setting, it requires the light to penetrate through a large volume of tissue for bigger patients. An alternative is to insert a diffusion probe directly into the patients lung, possibly while intubated in intensive care to illuminate internally. This method requires the light to penetrate less tissue allowing for larger geometries.

During two days, measurements were performed on a total of four porcine lungs. Different measurements were performed on each lung, due to the quality of the lung deteriorating over time. Both the drying out of the lung, but also the risk for alveoli walls breaking and merging alveoli, loosing the porous nature of the lung tissue. Table 4.2 shows what measurements were done on each of the lungs. Note that lungs 2,3 and 4 were being measured on the same day while lung 1 was measured on a week before. The measurements on lung 1 were used to perfect the method, while the data analysis is performed on lungs 2-4.

Table 4.2: Which measurements were taken on the four different lungs.

Type of measurement	Lung 1	Lung 2	Lung 3	Lung 4
External without pork padding	x	x		x
External with pork padding	x	x		x
Internal without pork padding	x		x	
Internal with pork padding	x		x	

To gain insight into where on the lung the measurements were taken, the lung lobes are numbered as shown in Figure 4.4. A crucial difference between human and porcine lungs is the addition of an additional lobe in porcine lungs in the sagittal plane (lobe 5). In actuality, the porcine lungs have a total of 7 lung lobes, 1 and 4 in the figure being split. However, since the measurements were taken closer toward the center line, the lobes can be regarded as one.

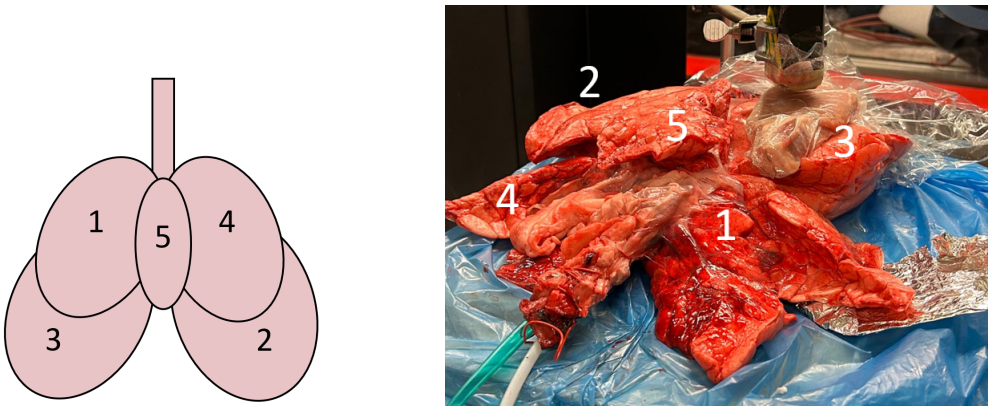

(a) (b)

Figure 4.4: A schematic picture showing the lobes of the porcine lung (a) and a picture of the lung (b) with labels to indicate lobe numbers.

Due to the sheer volume of the porcine lung measurements, each lung measurement will be assigned a code which describes the measurement.

- **First position**: The first position in the code indicates which lung the measurements is taken on 1,2,3 or 4.
- **Second position**: The second position indicates if it is an internal or external illumination. I for internal and E for external.
- **Third position:** Indicates which lobe number the measurement is taken on, in accordance with Figure 4.4.
- **Fourth position:** Indicates how many centimeters of pork were used as absorption padding.

An example of a code is 1E30 which indicates an external illumination on the first lung on lobe 3 without pork. Below is a list of each measurement that was done for each lung in code.

- **Lung 1:** 1E10, 1E12, 1E14, 1I30 and 1I32. Which denotes three series of external illumination on lobe 1 with different thickness of pork padding and two series of internal illumination on lobe 3 with

different thickness of pork padding. Since the signals obtained have a very different form than the others. Lung 1 will not be used for analysis.

- **Lung 2:** 2E10, 2E12 and 2E14. Which denotes three series of external illumination on lobe 1 with different thickness of pork padding.
- **Lung 3:** 3I30, 3I32 and 3I34. Which denotes three series of internal illumination on lobe 3 with different thickness of pork padding.
- **Lung 4:** 4E20. Which denotes one series of external illumination on lobe 2 without pork padding.

Assessing the lung tissue thickness was difficult, due to the irregular shape of the lung, as well as a difference in thickness due to level of inflation. It was also complicated further during internal illumination due to not knowing where the probe was located and the wall of the lung being difficult to assess. For external measurement, however, a measurement of the lung tissue thickness was determined to be around 3 cm.

Results

While a full description of how the results in this section are calculated can be found in Appendix A.2, a brief description will be presented at the start of this section, along with examples of GASMAS signals.

Figure 4.5 shows two obtained GASMAS signals for measurements on Lung 2 without pork padding, the left when the lung was filled with pure oxygen gas, and the right when the lung was filled with pure nitrogen gas. Along with the signal, the linear regression was applied to the oxygen signal. It would be expected for the nitrogen signal to not exhibit a GASMAS signal due to the lack of oxygen gas present within the lungs. However, a small oxygen absorption can be found even in the signal obtained from the nitrogen filled lung. The reason for this will be discussed later in this chapter. When nitrogen-adjusting the signal, the GASMAS signal is divided by the value of the nitrogen gas signal as oppose to the linear regression. The adjustment is done due to to trying to assess if the GASMAS signal actually arises from the oxygen content in the lungs or if the signal is simply obtained due to other oxygen along the light path, weather it be from oxygen before the light enters the tissue or the light taking a path that circumvents the sample entirely.

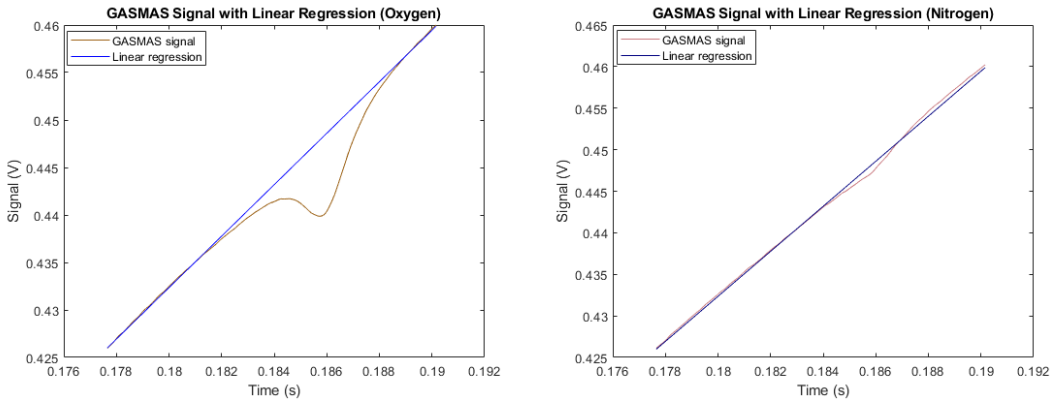

(a) (b)

Figure 4.5: The GASMAS signals obtained from measurements on lung 2, external illumination without pork padding, when the lung is filled with oxygen gas (a) and nitrogen gas (b) along with the linear regression obtained from the signal obtained during oxygen filling of the lung.

Table 4.3 shows the oxygen absorption calculated according to Appendix A.2 for the different lung measurements. The absorption and nitrogen-adjusted absorption are both presented for the measurements along with the difference between the two.

Table 4.3: The absorption in percent for the measurements for both the oxygen signal in relation to the linear fit and the oxygen signal in relation to the nitrogen signal.

Measurements	Absorption (%)	Absorption (%) (Nitrogen adjusted)	Difference
2E10(B.1)	1.81	1.59	0.22
2E12(B.2)	1.65	1.64	0.01
2E14(B.3)	1.19	0.59	0.6
3I30(B.4)	2.09	1.18	0.91
3I32(B.5)	1.70	1.14	0.56
3I34(B.6)	1.56	0.60	0.96
4E20(B.7)	1.68	1.32	0.36

The obtained absorption values can then be used together with the thickness of the pork padding to show its dependence on the thickness. When the absorption is not adjusted with the nitrogen signal, the absorption shows a linear dependence with the pork padding, demonstrated below.

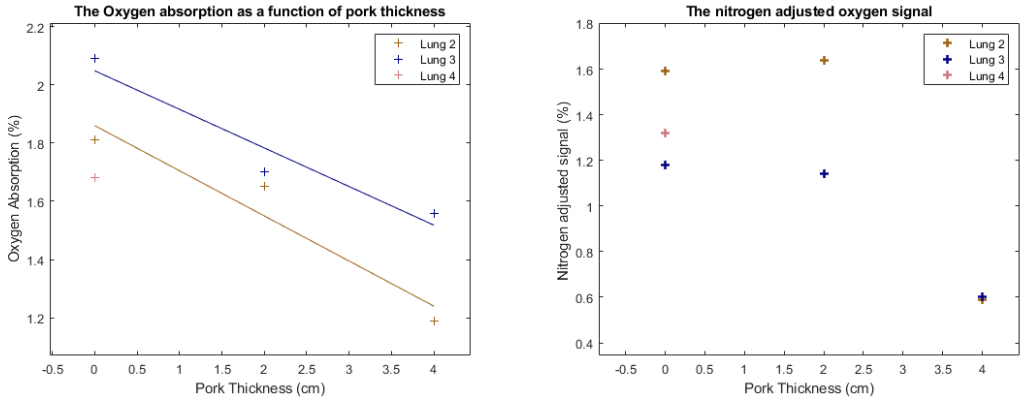

(a) (b)

Figure 4.6: The absorption in percent as a function of the pork thickness for the three lungs. The unadjusted oxygen signal along with linear regressions for lung 2 and 3. The resulting slopes of the measurements are -0.155 for lung 2 and -0.133 for lung 3 (a). The nitrogen adjusted signal for the three lungs (b).

4.1.3 Discussion

As was explained in the theory section, the absorption can be used to calculated the equivalent mean path-length of the light through the gas. Simulations translates the selected absorption peak to a mean path-length for both 100% and 21% oxygen, shown i figure 4.7.

Absorption values obtained from pork encased extruded polystyrene foam exhibit an oxygen absorption signal of around 2% for 2.5 cm of extruded polystyrene foam and around 4.5% for 5 cm of extruded polystyrene foam (excluding last measurement). While precise values of the equivalent mean path-lengths cannot be exactly determined due to the uncertainty in absorption. By using the Beer-Lambert law for the selected peak for 21% oxygen gas, this absorption results in a path length of 74 cm for 2.5 cm extruded polystyrene foam and 169 cm for 5 cm extruded polystyrene foam.

Similarly, the pure oxygen simulations can be used to find the mean equivalent path-length in the porcine lung measurements. The mean value of the absorption for all of the lung measurements is 1.67% which translates to 13 cm in pure oxygen. While the mean equivalent path-length of the porcine lung measurements is significantly reduced, the values show that scattering inside the tissue is present due to the mean equivalent path-length being longer than the thickness of the sample, being only a few cm in length.

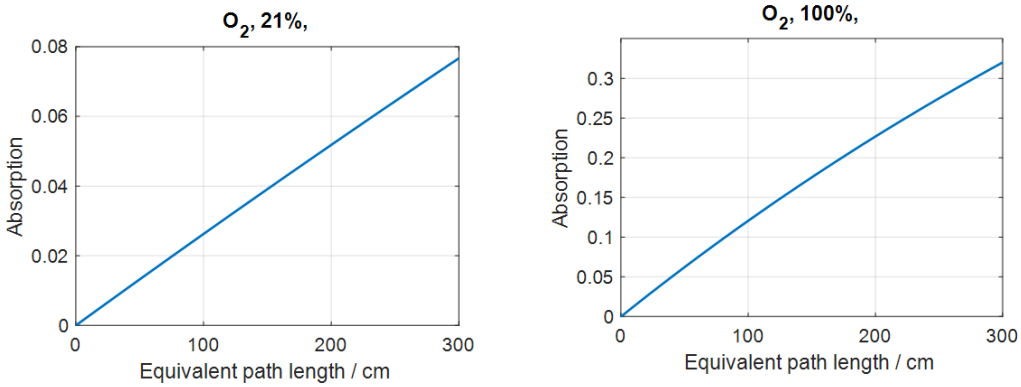

(a) (b)

Figure 4.7: Simulations performed by Anna-Lena Sahlberg showing the absorption as a function of light path-length. For the selected light frequency for oxygen gas 21% (a) and 100% (b).

Extruded Polystyrene Foam Pork Models

When adding pork to the extruded polystyrene foam, it is to be expected that the oxygen absorption signal should remain constant, while the transmission of light through the sample decreases. This is due to the fact that no porous material is added but rather absorbing material. The effective path-length of the light through the gaseous pores of the extruded polystyrene foam should not be extended, and therefore the absorption should remain the same. This expectation holds true for the two thickness of extruded polystyrene foam ($\sim$ 2.1 % for 2.5 cm of extruded polystyrene foam and $\sim$ 4.5 % for 5 cm of extruded polystyrene foam) with the exception of the last measurement. That this measurement is an outlier could be due to the fact that light might have taken another path through the sample reducing the effective path-length. When the collected light is reduced, the effects of light taking an unintended path may be increased, such as circumnavigating the extruded polystyrene foam by reflecting on a surface in the room. Since the padding is so thick, another measurement was taken when the setup was shielded by a black cloth, which exhibits an absorption of 3.2 %, which is still a reduction from the mean of 4.5 % for the rest of the measurements, but shows the impact of stray light.

It is also observed that the absorption for 5 cm extruded polystyrene foam is bigger than for the 2.5 cm extruded polystyrene foam. This is not surprising since the effective path-length needed to penetrate the thicker sample of extruded polystyrene foam is longer than for the thin sample of extruded polystyrene foam.

Porcine Lung Models

When assessing the absorption in the porcine models, values from different measurement series (i.e different lungs or lobes) cannot be directly compared. This is mainly due to the fact that the lungs are quite different. Both the volume probed, porosity and overall lung differences may impact the measurements. Comparisons between different thickness of pork padding for the same lobe and method is the best way to determine if this value is constant.

Generally it can be observed that the absorption signal gets reduced as pork padding is added. The change is small, averaging -0.155 for lung 2 and -0.133 for lung 3 per cm pork adding. While this should ideally not be the case, the main reason is expected to be that when the extra weight that is present when pork padding is added, it inhibits the lung from inflating to its maximum volume, reducing the equivalent path length through the lung tissue and thereby the absorption.

There is an interesting pattern that appeared when observing the oxygen signal when it is adjusted with the nitrogen signal. Showing the same value for 0 and 2 cm of pork and decreasing for 4 cm of pork. The two lungs follow a similar pattern. It is difficult to assess why this pattern may appear, since it is present in both of the lungs it might not be a coincidence. The reduction in signal when applying 4 cm of pork is evident in the unadjusted signal but is more dramatic in the adjusted signal. The most probable explanation is that when pork padding is applied it is harder to ventilate the lung due to the weight of the pork, resulting in a gas composition that is not solely nitrogen or oxygen for the two measurements, the oxygen content of the nitrogen measurements creates a signal resulting in the adjusted signal being low.

Improvements

There are some improvements that can be done to the absorption assessment. Ideally, more different thicknesses of extruded polystyrene foam should be utilized so that it can be assessed what kind of dependence the absorption has on the extruded polystyrene foam thickness. If continuing to use porcine lungs, they should be chosen so that the thickness is consistent over the measurements, as this will enable easier comparison between measurements. The lungs should also ideally be the same size and as fresh as possible, ensuring that the effect of lung differences on the signal is reduced. While the ventilation method worked well, as there is still an oxygen signal present in the lung when they were filled with nitrogen, it suggest that the oxygen was not completely flushed out of the lung. An alternative method for ensuring that the gas is entirely flushed out of the lung would be optimal to ensure a complete analysis.

The interference filter that is used in front of the detector may not be an optimal way to detect the signal. Interference filters are composed by a number of dielectric films that reflect unwanted light, however, the angle of incidence is of importance when interference filters are used. Since the signal that is obtained from the lungs is highly scattered, this filter may also filter out wanted light, reducing the signal obtained. If the interference filter were to be removed however, other methods will have to be employed to reduce the unwanted light.

While unwanted light is reduced with the interference filter unwanted signal can be attained from the laser taking a path that is not through the sample. Light may reflect on a surface in the room and return to the detector through another way, exhibiting an oxygen signal that is not coming from sample. This can be mitigated by shielding the detector by using a black cloth or paper, as was shown in the extruded polystyrene foam model measurements. Since the signals obtained when filling the lungs with nitrogen did show a considerably lower oxygen signal, we can confidently conclude that the vast majority of detected signal comes from light that has penetrated through the sample.

The lung quality is another aspect that complicates the measurements. As the lung dries out the elasticity is reduced, increasing the risk of ruptures in the tissue resulting in gas leaking out of the lung or causing rupture of the alveoli walls. This can affect or destroy the porous nature of the tissue merging the aveoli into a big gas filled balloon in the lung. While this process may reduce the effective path-length, reducing the oxygen absorption signal, since the porous property is no longer present, some of the absorbent tissue is removed, improving the light transmission.

Another improvement is to use a real diffuser probe for the measurements instead of creating our own. It is difficult to ensure that the make-shift diffuser probe has an even distribution of light in all directions and that light is not absorbed in the material, as well as assessing the output power.

4.2 Signal-to-Noise Ratio (SNR) - Assessment

The data that is obtained from the photodiode is recorded by the oscilloscope in four different forms which will be described below. To simplify the communication the signals will from this point be described using letters instead A,B, C and D.

- **Unprocessed signal (A-signal):** This signal denotes one signal sweep that is transmitted from the photodiode to the oscilloscope. While not representative of the entire series of measurements, it gives a qualitative representation of what might be instantaneously obtained in a clinical setting.
- **Time averaged signal (B-signal):** This signal is obtained by setting the oscilloscope to record an average of the A-signal over numerous sweeps. In this study, that average was over 300 signals being averaged over time. This improves the SNR of the signal considerably.
- **Moving average signal (C-signal):** This is the A-signal with a moving average filter applied to it during the data collection in the oscilloscope.
- **Averaged moving average signal (D-signal):** This signal is obtained by setting the oscilloscope to record an average of the C-signal over numerous sweeps. In this study, that average was over 300 signals being averaged over time. Similarly to the B-signal, this was shown to improve SNR.

These four signals were obtained for all the measurements. Figure 4.8 shows an example of the four different signals obtained, in this case one of the lung measurements.

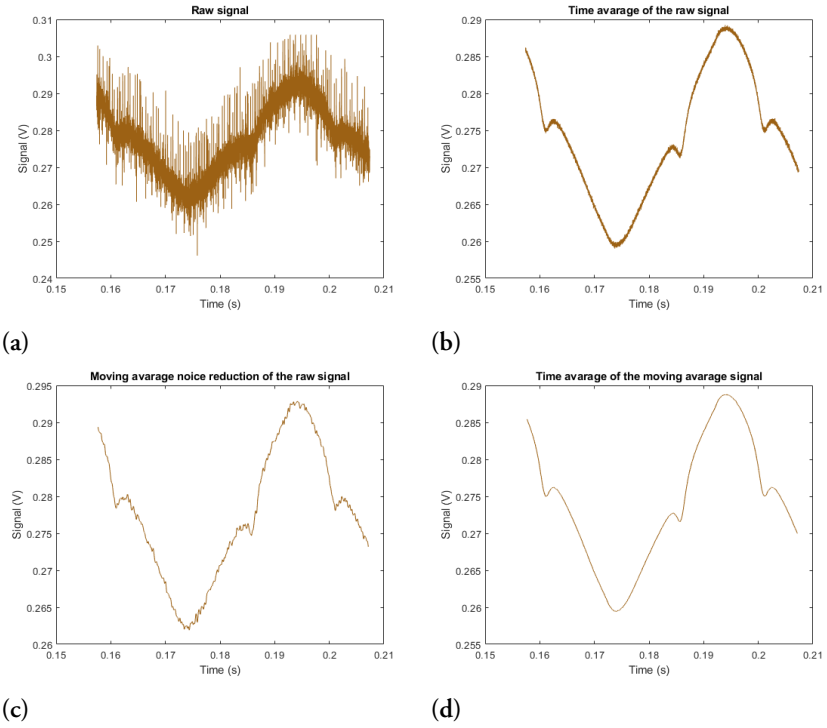

Figure 4.8: The four different signals that are obtained from the oscilloscope when measuring. The unprocessed signal (a), the time average of the A-signal (b), the moving average noise reduction of the A-signal (c) and the time average of the C-signal (d).

4.2.1 Results

Extruded Polystyrene Foam Pork Model Measurements

While the process of obtaining the SNR can be found in its entirety in Appendix A.2, the start of this section will feature some examples of the SNR for signals, enabling easier understanding of the results. Figure 4.9 shows the effects of both time averaging and absorbing pork padding on the SNR of the signal. The left graph shows the A- and the B-signal for 2E10, highlighting the positive effects of time averaging and the right graph shows two different A-signal, one from 2E10 and the other one for 2E14 highlighting the impact of absorption padding on the SNR of the signals.

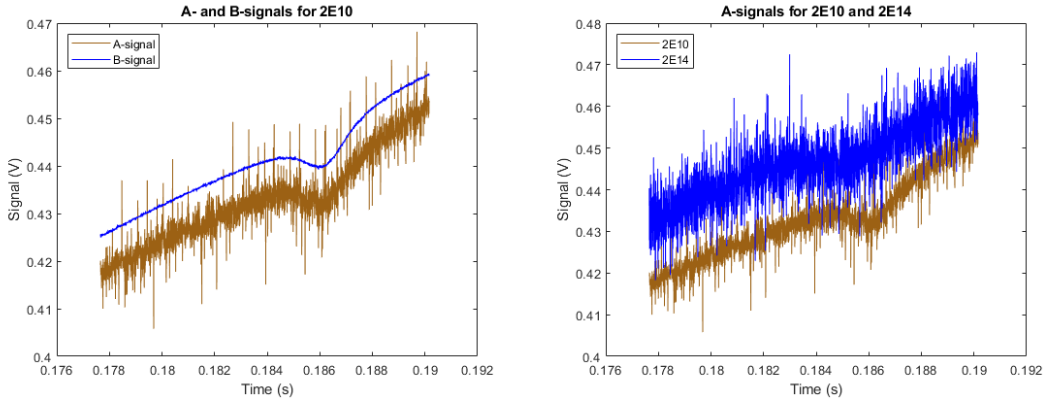

(a) (b)

Figure 4.9: The A- and B-signals obtained from measurement 2E10 (a) and the A-signals from the measurements 2E10 (brown) and 2E14 (blue) (b).

Table 4.4 shows the SNR for the four different signals, calculated according to Appendix A.3. The pork thickness is applied in the order described in figure 4.1.

Table 4.4: The SNR for the different signals for different extruded polystyrene foam pork measurements, calculated according with Appendix A.3. A zero denotes that the signal was not legible.

Extruded polystyrene foam thickness (cm)	Pork thickness (cm)	A-signal	B-signal	C-signal	D-signal
2.5	0	12.4	186	100	413
2.5	2	4.46	72.5	27.8	266
2.5	4	3.42	53.2	40.5	279
2.5	6	0.77	10.0	4.88	63.7
2.5	8	0	1.48	0	13.3
5	0	29.7	500	231	366
5	2	7.16	146	67.4	541
5	4	2.37	56.8	23.6	521
5	6	0	4.43	0	37.7
5	8	0	6.71	3.37	21.1

While all of the signals are of importance, focus will be placed on the D-signal which shows the best SNR and the C-signal which gives momentary view of the signal while maintaining a high SNR. Figure 4.10 shows the SNR for the C-signal (left) and D-signal (right) are shown as a function of pork padding thickness. The brown line shows the values obtained for 2.5 cm of extruded polystyrene foam and the blue line for 5 cm of extruded polystyrene foam.

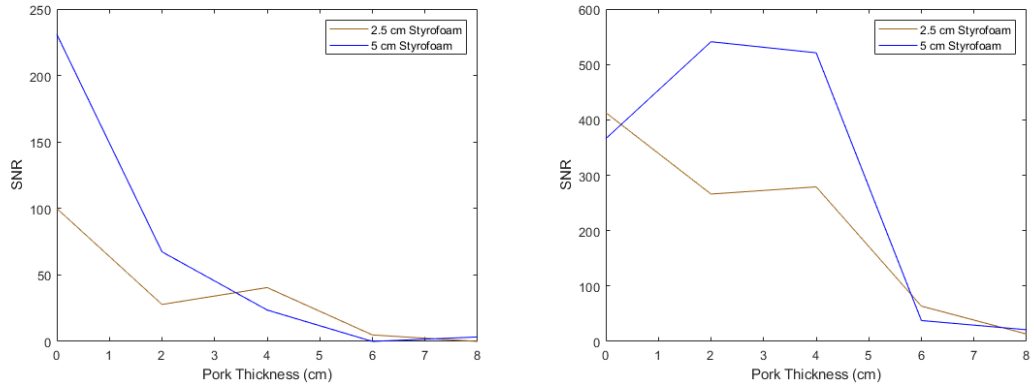

Figure 4.10: The SNR from the C-signal (a) and the D-signal (b) calculated according to Appendix A.3on two blocks of extruded polystyrene foam of different thickness (2.5 and 5 cm) with different thickness of pork padding added.

The C-signal SNR can be fitted with an exponential function, showing a clear exponential dependence for the 5 cm extruded polystyrene foam measurements. Figure 4.11 shows the exponential fit along with the SNR values obtained.

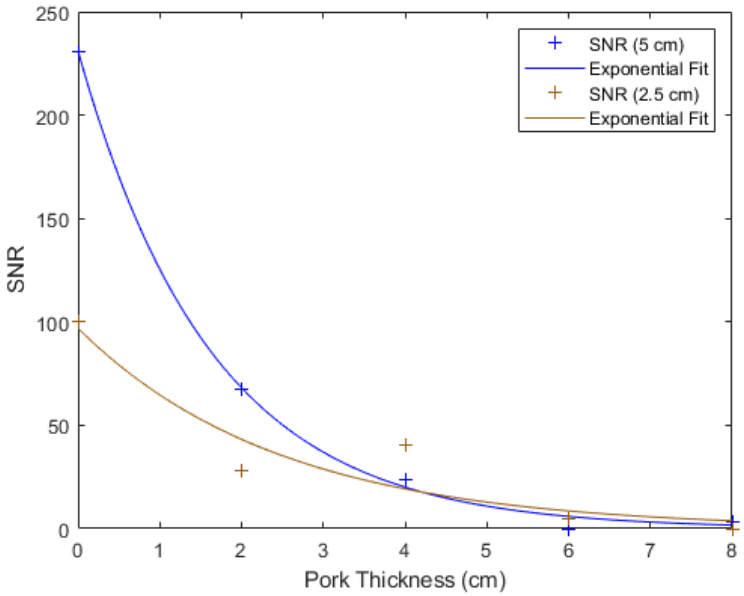

Figure 4.11: The SNR from the C-signal calculated according to Appendix A.3on two blocks of extruded polystyrene foam of different thickness (2.5 and 5 cm) with different thickness of pork padding added, along with an exponential fit.

Porcine Lung Measurements

Table 4.5 shows the obtained value for SNR for the four different signals obtained from the porcine lung measurements, calculated according to Appendix A.3. An explanation to the code assigned to the measurements can be found in Section 4.1.2.

Table 4.5: The SNR for the different signals for different porcine lung measurements, calculated according to Appendix A.3. A zero denotes that the signal was not legible. The last line shows the mean for each signal.

Measurements	A-signal	B-signal	C-signal	D-signal
2E10	1.82	30.2	22.57	379
2E12	0.80	14.6	14.2	60.3
2E14	0.92	16.56	7.44	79.5
3I30	0.43	5.09	3.42	53.1
3I32	0.45	5.83	6.63	64.4
3I34	0	2.80	0	33.5
4E20	1.77	21.8	14.0	143
Mean	0.88	13.84	9.75	116

Figure 4.12 shows the SNR for the C-signal (left) and D-signal (right) are shown as a function of pork padding thickness.

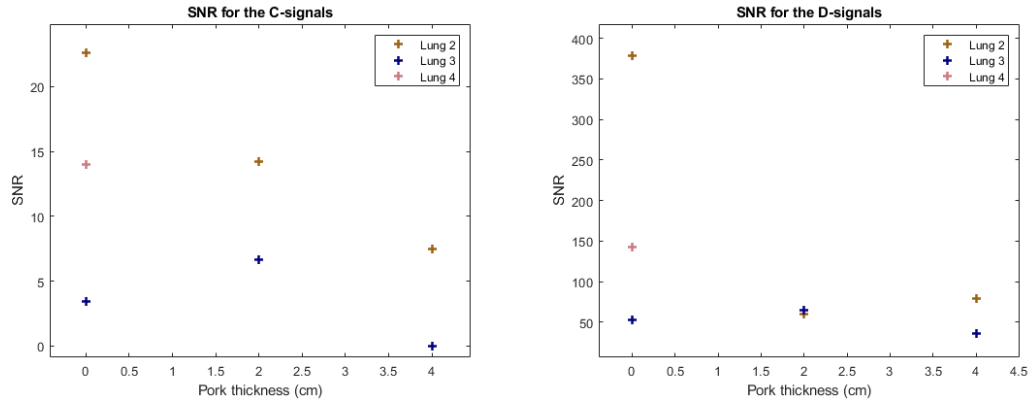

(a) (b)

Figure 4.12: The SNR from the C-signal (a) and the D-signal (b) calculated according to Appendix A.3. Lung 2 and 4 had external illumination and lung 3 had internal illumination.

4.2.2 Discussion

There are some hypothesis that can be made about the results and what properties they should exhibit. The SNR should be reduced when pork padding is placed in front of the detector. This is due to a reduction in incoming photons which reducing the amplitude of the signal, while maintaining the noise. It is assumed that a time averaging of the signal should result in an improved SNR. The SNR for the B and the D signals should also show an improvement to the SNR for the A and C signals, due to the B signal being a time averaging of the A signal and the D signal being a time averaging of the C signal. Furthermore, the C signal should have a higher SNR than the A signal, due to being a moving average of the A-signal and the D-signal should have a higher SNR than the B-signal for the same reason.

For the SNR values the signals are obtained in very different ways. Both the A and the C signals are continuous and instantaneous signals. While they can appear noisy, they give a momentary signal indicating the absorption at the exact time. The SNR values for these signals should therefore be seen as an indicator of potential applications rather then a systematic investigation. The SNR may also fluctuate rapidly in these signals over the measurement, making these values uncertain.

Extruded Polystyrene Foam Pork Model

For the extruded polystyrene foam pork measurements the SNR for the D-signal behave in a peculiar way, increasing when the pork thickness is increased. While this behaviour may seem strange, these values make very little difference since they are so high. The main point of interest is the detectability which is clear for the measurements. As is to be expected, the SNR is generally higher for the 5 cm thick block, this is due to the absorption being higher for these measurements, resulting in a higher SNR for the same noise. This trend is broken for higher pork thickness where the 2.5 cm block has a higher SNR. This may be due to that the thicker extruded polystyrene foam reduce the incoming light to the detector due to scattering making the noise present more prominent.

The exponential fit shown in figure 4.11, while accurate for the 5 cm thick extruded polystyrene foam measurements are not as precise for the 2.5 cm extruded polystyrene foam measurements. A exponential decrease is not surprising, since it can be seen as an exponential decrease in light registered by the detector due to the Beer-Lambert law. Caution must be practised when making this analogy, however, since the Beer-Lambert law assumes minimal scattering, and our medium is highly scattering. There exists however alternative versions of the Beer-Lambert law that includes both scattering and anisotropy in its formula while still having the exponential decrease in signal through the material, which is probably what is observed here. That the 2.5 cm extruded polystyrene foam does not follow this pattern as closely is likely due to the C-signal being instantaneous, and may therefore fluctuate between measurements.

Porcine Lung Models

The SNR for both the C and the D signal in the lung measurements show a high level of promise for future applications. Exhibiting quite high SNR, even when the added pork padding is thick. This indicates that even when the signal is lower, such as the case would be if the lung was filled with air, the signal would still be visible. Since air is composed of approximately 21% oxygen, the SNR would be decreased to 21%, compared to the signal obtained when the lung was filled with pure oxygen. Figure 4.13 shows the D-signal for the external illumination (left) and internal illumination (right) with the thickest pork padding of 4 cm. The signal is clearly visible, even without any processing.

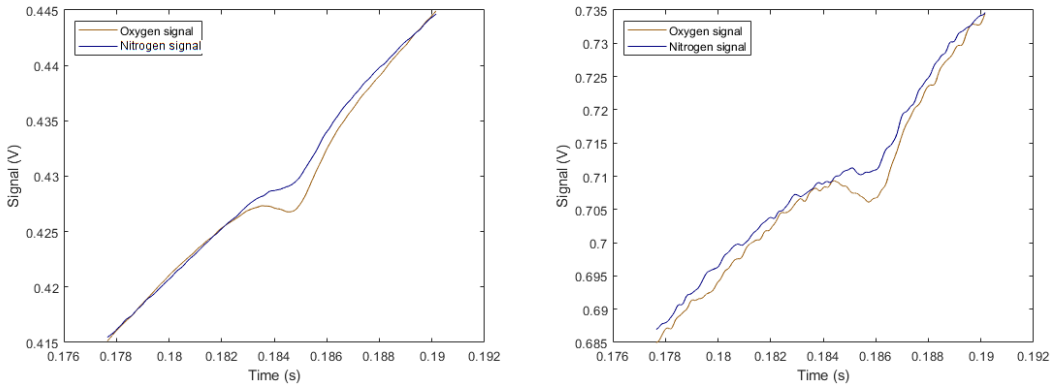

(a) (b)

Figure 4.13: The D-signal from 2E14 (a) and 3I34 (b) showing the signal both during pure oxygen ventilation and pure nitrogen ventilation.

For the C-signal for lung 2 (external illumination) the SNR decrease seem to be very linearly decreasing while lung 3 is much less linear. While this is quite surprising, exhibiting a different dependence than the extruded polystyrene foam measurements, this can still be used to approximate how an increase in pork padding would effect the SNR. If it is to be assumed that a SNR of 2 is needed to obtain a signal, the

signal would be visible even with a pork thickness maximum of 5.37 cm. If the SNR is allowed to be 1, a thickness of 5.63 is the maximum. If an exponential fit were to be performed instead, and the limit were to be set at an SNR of 2, a thickness of 9.3 cm of pork padding would be allowed. If the SNR is instead set to 1, a thickness of 12 cm would be allowed. Figure 4.14 shows the values along with a linear and a exponential fit. Due to the uncertainty in the values for the SNR of the C-signal, it is unwise to extrapolate to much from the obtained values. Furthermore, the measurements are performed using pure oxygen gas, which is seldom what lungs in clinical settings are ventilated with. Both of these models only serve to show that the thickness of the pork could be expanded, and still allow for a signal to be detected.

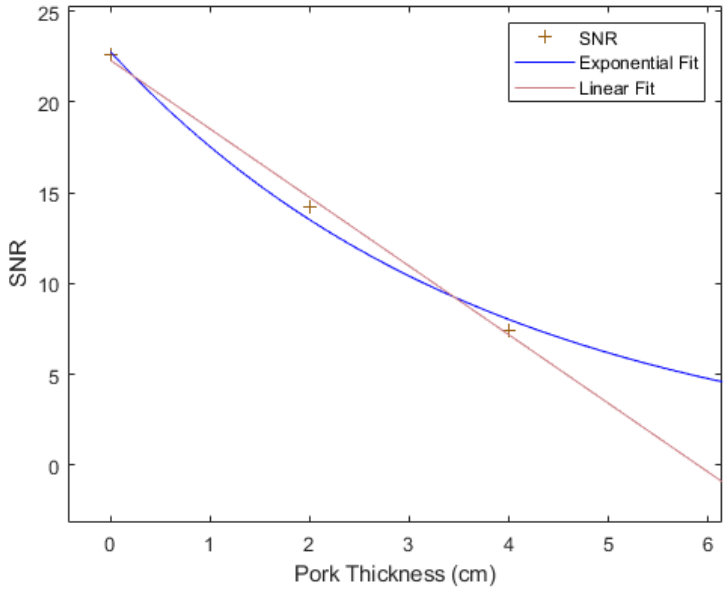

Figure 4.14: The calculated SNR for the C-signal of lung 2, along with a linear and an exponential fit.

In Lewander et al. (2011)[21] the diameter of a 27 week preterm infant was determined to be 6 cm and the correspondent value for a full-born infant was 10 cm with a typical chest wall thickness of 0.6 and 1.2 cm respectively. Combining these values with the SNR values obtained in the lung measurements shows that clinical implementation to full-born infant is viable, even giving room for diagnostics on bigger infants. While pork is not a perfect approximation of human tissue, these results show the potential in the method.

It can also be observed that it is quite effective to apply a moving average filter for the signal to ensure optimal SNR for the measurement. This is indicated by an improvement in SNR for the moving time average smoothing of the signals.

Improvements

A way to improve SNR for the measurements is to use Wavelength Modulation Spectroscopy (WMS). This technique utilizes a frequency generator and a lock-in amplifier to reduce noise. The wavelength is modulated at a high frequency and the lock-in amplifier filters out anything that is not at that modulation frequency. The reason for this method being so powerful is that noise that is present in the signal is usually low frequency. While this method was initially planned to be used, when operating the setup, the noise seemed to increase instead of decreasing. Further investigations should utilize this technique to ensure that a upper limit for absorption padding can be established.

Chapter 5

Evaluating Skin Heat Development During Laser Illumination

In expanding the potential for GASMAS lung diagnostics, the power of the administered light has to be increased. This brings about the challenge of heating, which can cause damage to the tissue, and thereby the patient if not held sufficiently low. In this chapter, the heating during light illumination will be evaluated. Using different illumination methods, power, area and skin tone.

5.1 Method

Free Beam Measurements

For the free beam measurements six different volunteers were measured on, varying in skin tone. To assess skin tone the Fitzpatrick scale is used, categorizing skin color into 6 different categories, where 1 is the palest and 6 is the darkest. The values of the volunteers measured on where assigned the values 2,2,3,3,4 and 6. This assessment was however not done by a medical doctor and may not accurately reflect what would be determined by a professional. The measured temperature was always held under 43 °C to avoid any potential tissue damage. The first measurement, was therefore performed at a moderate power to then evaluate the power needed for the other measurements. The power differed from a minimum of 50 mW to a maximum of 800 mW.

Below the method will be described in steps.

- **Ensuring correct beam qualities:** The first step was to ensure that both the size and the power of the beam was correct for the measurements. This was achieved by first adjusting the lenses to ensure that the beam was close to collimated to ensure that there are no variations in illumination area if the arm was to be moved slightly. To ensure that the light illuminated the correct area, a target is used and lenses adjusted until the beam is in the middle. Afterwards the aperture is used to ensure correct area of the beam. For the measurements on different volunteers the illuminated area was circular with a size of 1 cm in diameter. Finally the power meter was placed in the beam-path and the output coupler from the laser was tuned to ensure the correct power.
- **Measurements:** Figure 3.4 shows a schematic picture of the setup used. The arm was placed in the holder while the laser was blocked and the thermal camera was put in place. When the laser was

unblocked, a stopwatch was started. Every 30 seconds the temperature of the spot that was illuminated was recorded as well as a reference point on a place where the light did not illuminate the skin. Between measurements using different power levels the skin was left to completely cool down which was ensured by utilizing the heat camera. The duration of the cooling differed. The illumination lasted for a duration of 5 minutes per power level. The time was chosen after observing that a constant temperature was achieved after around 4 minutes, see Figure 5.1.

As well as measuring on different skin tones, the effect of the area of illumination was evaluated by measurements performed on the author, illuminating with 300 mW in power with a circular circular illumination area with 0.5, 1, 1.5 and 2 cm in diameter.

Probe Measurements

The same procedure that was done on the free beam was performed for the probe. It was, however, observed that the heating was stronger with probe illumination, resulting in generally lower power used for these measurements.

5.2 Results

While measurements for both the free beam and the probe measurement were taken on a total of six volunteers, the measurements on a singular volunteer will be used to first demonstrate the appearance of the results, ensuring that the results are clearly understood when compiled.

Figure 5.1 shows the results obtained from measurements on one of the volunteers. Since the most interesting quantities are the difference in temperature between the illuminated area and the reference area, this is the value that will be demonstrated.

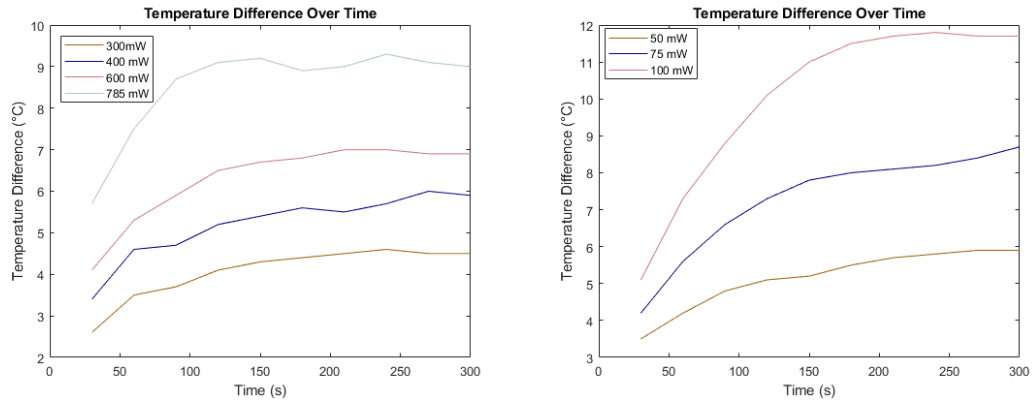

(a) (b)

Figure 5.1: The temperature difference in °C between the illuminated area and the reference area as a function of time for different illumination powers using free beam illumination (a) and probe illumination (b).

The maximum difference in temperature shown in 5.1 is then used to obtain the maximum temperature difference as a function of power. A linear regression is created showing the linear relation between the illumination power and maximum temperature difference.

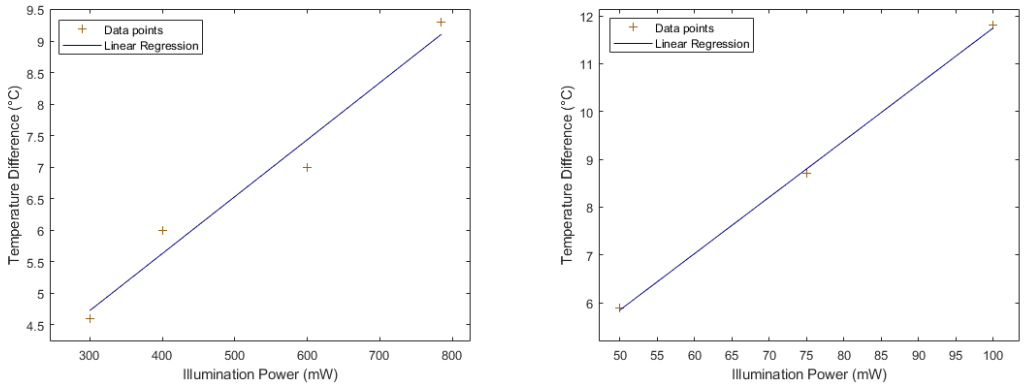

(a) (b)

Figure 5.2: The maximum temperature difference in °C between the illuminated area and the reference area as a function of illumination power using free beam illumination (a) and probe illumination (b), obtained from the data shown in Figure 5.1.

The process of linear regression described above and shown in 5.2 was performed for all of the volunteers measured on, resulting in 6 different linear regressions per illumination method, shown in Figure 5.3.

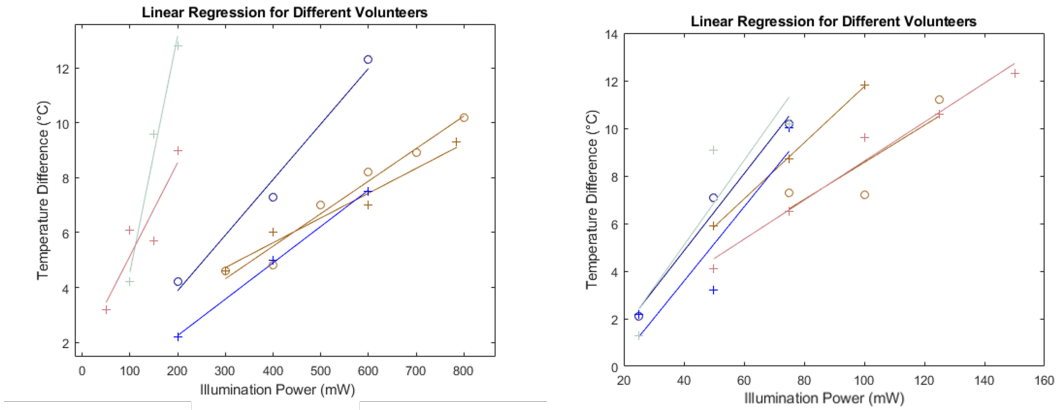

(a) (b)

Figure 5.3: The maximum temperature difference in °C between the illuminated area and the reference area as a function of illumination power for different volunteers including a linear regression for each volunteer. The color shows the volunteers value on the Fitzpatrick scale. Bronze: FP2, Blue: FP3, Pink: FP4 and Green: FP6. Illumination by free beam (a) and by probe (b).

Table 5.1 shows the slope coefficients for the linear relation between maximum temperature difference between the illuminated and reference, for all different volunteers. The letters indicate the different volunteers with the same Fitzpatrick scale value, the A is indicated by circular markers in Figure 5.3.

Table 5.1: The slope coefficients for the different volunteers measured on along with the Fitzpatrick scale value. The letters are to indicate which volunteer having the same Fitzpatrick value that the coefficient belongs to.

Fitzpatrick scale value	Coefficient (Free beam) (°C/W)	Coefficient (Probe) (°C/W)
2A	11.8	78
2B	9	118
3A	20.2	162
3B	13.2	156
4	34	82
6	86	178

These values were used to create two more linear regressions using the Fitzpatrick value for the x-axis.

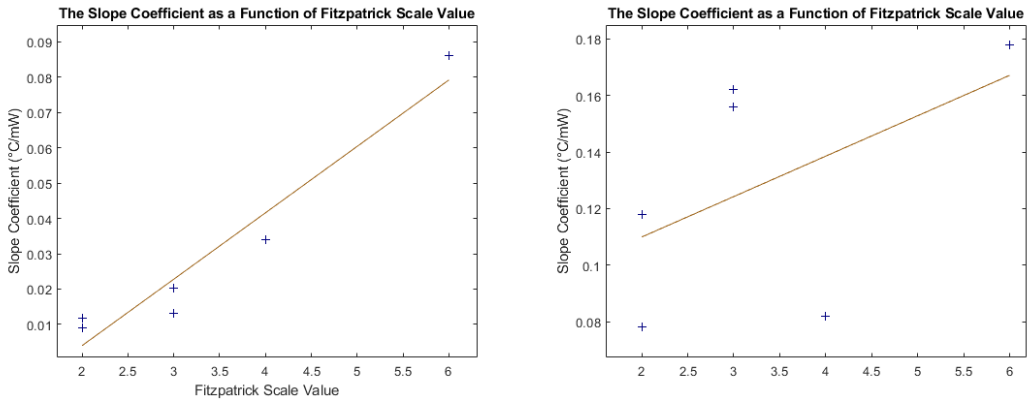

(a) (b)

Figure 5.4: The slope coefficients obtained from the linear regression of the maximum temperature difference as a function of power as a function of Fitzpatrick scale value along with a linear regression of these values for free beam illumination (a) and probe illumination (b).

Area measurements

Figure 5.5 shows the results obtained for the temperature raise for different areas of illumination. Both in terms of maximum temperature difference and the temperature difference over time.

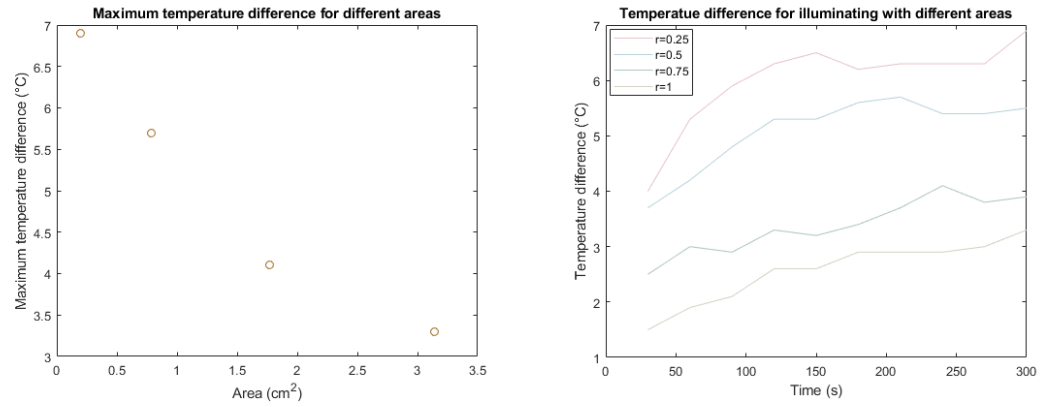

(a) (b)

Figure 5.5: The maximum temperature as a function of area illuminated (a) along with the temperature difference over time (b).

5.3 Discussion

As is clearly demonstrated in Figure 5.1 the illumination by probe results in a larger temperature increase in the illuminated area compared to illumination with a free beam at similar power. This is likely due to two main factors. The probe illuminates a considerably smaller area compared to the free beam (44 mm^2 and 79 mm^2) which in conjunction with the area measurements contribute to this difference, but not entirely. Comparing the temperature increase for a hypothetical illumination area of 44 mm^2 using the data obtained from the illumination area measurements, and the linear regression obtained from the probe measurements on the author, results in a maximum temperature difference of 6.36 °C for the free beam, and temperature difference of 24 °C for the probe.

The probe inhibits one of the mechanisms responsible for cooling, convection. The flow of air is important for the cooling of illuminated skin during the free beam measurements. When covering the area with the

probe and tape, this is not possible. While the target for theses measurements were to measure the temperature of the skin, it is possible that the probe itself also contributes to the warming of the skin as the probe itself gets heated by the laser. While the probe is not heavily absorbent it is still possible that it absorbs some of the light raising its temperature. This would then also impact the temperature difference in a way that is not dependent on skin tone.

It is clear that the maximum temperature increase predominantly follows a linear relation to the power of the light. This result is in accordance with the findings made by Molin in his 2018 thesis [9], but also previous studies on the topic using lower power [22]. The values do not, however, align perfectly on the straight line, which is to be expected. The body is complex, and processes cannot always be anticipated. The measurement method is also not entirely stationary, giving rise to small differences between measurements. The highly linear relation, is a practical feature in a clinical setting enabling a qualified guess of all possible illumination power. If the measurements are consistently linear, only one measurement is needed to assess the power dependence of the temperature. It is expected for the linear regression to exhibit a value of zero when the illumination power is zero, this is not the case for either of the linear regressions which may arise from inherent differences between the illumination and reference area.

Figure 5.3 clearly indicates that darker skin exhibits a higher temperature increase at lower powers. But more important is the slope of the linear regressions showing darker skin generally having a steeper slope. This difference is more noticeable for the free beam, showing a high raise for the volunteer with the Fitzpatrick scale value of 6 and the low slopes for both of the volunteers with a Fitzpatrick scale value of 2. While it can be observed that one of the type 3 volunteers had lower values for most intensities, the slope is still greater than the type 2 volunteers. The probe measurements are clearly more gathered, and the difference between skin types is not as clear. While the slopes for the free beam measurements has a clear increasing trend for darker skin tones, the slope values obtained from the probe measurements fluctuate, the volunteer the Fitzpatrick value of 4 having the second lowest slope, the cause of this will be discussed in the probe section below.

Free Beam Measurements

Figure 5.3 show that there is a clear linear relationship between the slope of the linear regression of the maximum temperature as a function of illumination power and the Fitzpatrick scale value for the free beam measurements. The Fitzpatrick scale cannot, however, show small skin tone differences, leaving nuance to be desired. There is no space between the numbers resulting in that skin tone might be over or under valued. The linear regression for the free beam measurements would, from this regression, become negative for type 1 skin, which is not representative of reality, since it would result in cooling the skin. Clearly more data is needed to get a model that represents reality. This clear dependence on skin tone is an important finding, highlighting the importance of taking skin tone into account when optical monitoring methods are considered in a clinical setting. The results also clearly indicate that tissue damage from heating is only of concern for very powerful lasers, even for CW lasers. Therapeutic applications with much lower power, such as current methods for neonatal infants which exhibits an illumination power of $\sim$ 20-30 mW, and do not have to take heating into account for their methods, but need to be observant if the prospect of expanding their patient pool to include bigger infants or children.

Probe Measurements

While the linear relationship to Fitzpatrick scale value is evident for the free probe measurements, the linearity is not as clear for the probe measurements. There are two measurements that are quite trend braking, 2A and 4. This is likely to be a consequence of the method used for assessing the power of the probe. The power meter (S425C Thermal power sensor, Thorlabs) that was utilized assesses the power by calculating

the heating of a surface related to the incident power of the laser. For finding the intensity, the probe is placed very lose to the power meter and then tuned to the correct power. The first two measurements 2A and 4 were done without any issue. However, afterwards it was noted that just holding the probe close to the power meter without any light enabled shows a power. This is likely due to the probe being heated during the measurement, when placed close to the power meter, the heat is likely transferred. In turn this results in a lower tuning of the power from the probe, since the probe heat contributes to the power shown. As the heat increases with intensity, this effect gets bigger for higher powers, scaling with power. The intensity then becomes lower than listed, resulting in a flatter slope. For the following measurements, the probe was cooled down between power levels mitigating this effect. If the outlying values were to be disregarded, a new linear regression can be made, shown in figure 5.6. While still not entirely linear, a clearer linear relation is exhibited.

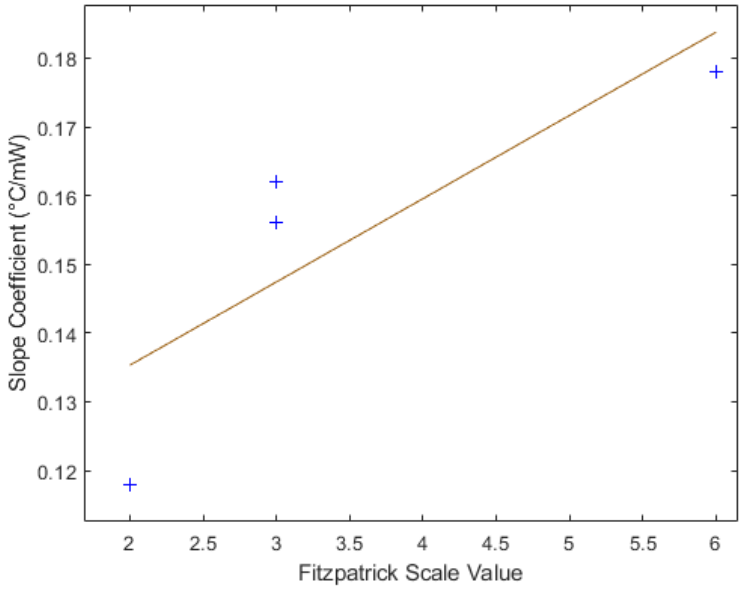

Figure 5.6: Caption

Another contributing factor might be the impacted cooling mechanisms. The convection is reduced, allowing for other cooling mechanism to have an increased importance. Blood flow might be an impacting factor, and may differ between the volunteers. Further measurements will be needed for a clearer picture.

Area Measurements

It is difficult to anticipate what form these measurements would take before the experiment was done. The only aspect that was certain is that reducing the area with constant power would increase the heating and vice versa, since the intensity of the light increases. Finding a theoretical model for the heating process is complex due to the body being a complex thermodynamics system. The reason for this complexity is that with increased area, the convection to the surrounding air and the conduction to nearby tissue increases. The heat transportation due to blood flow also impacts the cooling may also increase as a consequence of the increased area.

Improvements

There are some improvements that can be done to the measurement method for the free beam measurements. The first improvement that can be made is to evaluate and ensure beam quality. Currently the

beam profile is largely unknown, visually it is flat, but there could be some fluctuations in intensity over the beam profile. It would be beneficial to have a device that can both measure the power of the beam as well as the beam profile to ensure a flat intensity profile. The illuminated area and the reference areas were also chosen somewhat arbitrary. To ensure that the same spot is used for illumination and the same spot is used for reference between different volunteers, a standard can be created using the length of the forearm and a fraction could be used.

To improve the probe measurements it would be beneficial to get a better way to measure the power emitted from the probe. Currently the probe is placed in front of a power meter and the output coupling is tuned to determine the power. This method however is highly dependent on how the probe is placed. The power meter works by evaluating the heat that the light causes on the detector. If the probe is heated it might impact the power displayed on the power meter. In the experiments, the probe power was always measured in the same way which is why we are confident that it at least scales in the correct way, however the exact quantity of the power is not something that we can be confident in. To improve this, a power meter that can assess power over an integrated sphere would be a suitable way to determine the power.

To gain more insight into how the illumination area impacts the heating of the skin, area measurements should be performed on numerous volunteers. Even alternative emitter probes could be used to see difference in probe illumination for different illumination areas.

Chapter 6

Conclusion & Future Research

This thesis should be considered a proof of concept for higher powered GASMAS for lung monitoring, encouraging further research into the subject, showing that further research would be valuable. The results within themselves may not contribute significantly to any conclusions that might be applied in a clinical setting, but rather as a motivation and basis for further research.

6.1 GASMAS Signal Evaluations - Models and Porcine Lung Measurements

6.1.1 Conclusion

The results show that we can see a clear oxygen gas absorption, with a high SNR for the GASMAS signal through a piece of porcine lung tissue with relatively thick pork padding shows promise in future clinical applications. The extruded polystyrene foam pork models shows promise in assessing the decrease in SNR as a function of absorber padding giving insight into the potential limitations of future clinical applications.

Assessing the differences and potential of using both external and internal illumination provided insight into the flexibility of the method and the potential in expanding the patient profile.

6.1.2 Future Research

The success of the porcine lung measurements indicate that the next step is to expand the measurements to living, sedated pigs. Both internal and external measurements could be made to further explore if this technique can be implemented on human patients. Investigating the intensity of the light would also be an interesting expansion, assessing how the intensity of the light transmission changes the signal and SNR. This is a pivotal investigation since in therapeutic applications the intensity of the laser should be held as low as possible while still gaining a good signal. Both due to the potential heating, but also to allow for cheaper lasers and less risk in terms of laser safety. It would also be interesting to do more porcine lung measurements with the improvements listed in the discussion section, including a more consistent lung quality and a professional diffusion probe.

6.2 Evaluating Skin Heat Development During Laser Illumination

6.2.1 Conclusion

In this thesis, an effective way of assessing skin heating caused by a certain wavelength of laser illumination was established. It was found that the skin heating linearly depends on the incident power, that the illumination area plays a central roll in the heat development and that skin tone has a large impact on the heat development.

The Fitzpatrick scale was utilized to find a linear relationship between the slope of the maximum temperature increase as a function of illumination power highlighting skin tone as an important factor for future research.

The illumination method, free beam or optical probe illumination, showed a central difference in heating, partially due to the reduced area for the probe illumination, but also due to insulation provided by the probe, affecting the cooling mechanisms of the skin.

For clinical applications of high powered laser illumination, the area should be expanded to allow for maximum light administration while reducing the potential challenges of heating.

6.2.2 Future Research

Generally for the heat measurements, it would be beneficial to conduct a clinical study using a similar protocol as done in this thesis. More patient parameters should be recorded to insure that the result comes from the source that we are investigating. Factors such as body weight, length etc. could be contributing factors. A dermatologist should also be included in the study to ensure that the patients are assessed correctly on the Fitzpatrick scale. A large amount of people of different skin tones may be necessary to obtain a result that is statistically significant.

In the thesis by Molin (2020)[9] the inner lip was used to mimic the properties of the inner lung, which is another part that can be included in the study. Alternatively, internal illuminations can be used on sedated pigs and a thermometry system could be used to assess heating in vivo inside the lung.

While the laser frequency that is used is of the most interest for the application at hand. I believe that further research should investigate how different wavelengths heat the skin, if a pattern can be established for different wavelengths, area of illumination, skin tone and power, then all possible therapeutic applications of laser light illuminating skin should be covered. It would be beneficial to create scale that replaces the Fitzpatrick scale when it comes to laser illumination on skin, where skin type is quantified by temperature increase instead of tone.

Bibliography

[1] Paul Zarogoulidis et al. "Pneumothorax: from definition to diagnosis and treatment." In: *Journal of thoracic disease* 6 (Suppl 4 Oct. 2014), S372–6. ISSN: 2072-1439. DOI: 10.3978/j.issn.2072-1439.2014.09.24. URL: http://www.ncbi.nlm.nih.gov/pubmed/25337391http://www.pubmedcentral.nih.gov/articlerender.fcgi?artid=PMC4203989.

[2] D. G. Peroni and A. L. Boner. "Atelectasis: Mechanisms, diagnosis and management". In: *Paediatric Respiratory Reviews* 1 (3 2000), pp. 274–278. ISSN: 15260550. DOI: 10.1054/prrv.2000.0059.

[3] Martin Hansson Tetiana Kovtiukh. *Neola Medical White Paper*. https://www.neolamedical.se/wp-content/uploads/White-paper-April-2023-R.pdf. 2023.

[4] "Diode laser spectroscopy for noninvasive monitoring of oxygen in the lungs of newborn infants". In: *Pediatric Research* 79 (4 Apr. 2016), pp. 621–628. ISSN: 15300447. DOI: 10.1038/pr.2015.267.

[5] Emilie Krite Svanberg et al. "Changes in pulmonary oxygen content are detectable with laser absorption spectroscopy: proof of concept in newborn piglets". In: *Pediatric Research* 89 (4 Mar. 2021), pp. 823–829. ISSN: 15300447. DOI: 10.1038/s41390-020-0971-x.

[6] Yueyu Lin et al. "Gas in scattering media absorption spectroscopy on small and large scales: Toward the extension of lung spectroscopic monitoring to adults". In: *Translational Biophotonics* 3 (3 Aug. 2021). ISSN: 2627-1850. DOI: 10.1002/tbio.202100003.

[7] Brandt, Anna. *Gas in Scattering Media Absorption Spectroscopy in Large Geometries: Towards Monitoring Oxygen in Adult Lungs*. eng. Student Paper. 2022.

[8] Hjörneby, Emma. *Simulations and modeling of light propagation in biological tissue*. eng. Student Paper. 2023.

[9] Molin, Martin. *In-vivo assessment of unwanted tissue heating during near infrared laser light emission*. eng. Student Paper. 2020.

[10] Sune Svanberg. *Atomic and Molecular Spectroscopy: Basic Aspects and Practical Applications - 4th Edition*. Springer International Publishing, 2003.

[11] Caroline Boudoux. *Fundamentals of Biomedical Optics*. Dec. 2016. ISBN: 9781366451194.

[12] M. Sjöholm et al. "Analysis of gas dispersed in scattering media". In: *Opt. Lett.* 26.1 (2001), pp. 16–18. DOI: 10.1364/OL.26.000016. URL: https://opg.optica.org/ol/abstract.cfm?URI=ol-26-1-16.

[13] A.C Eckbreth. *Laser Diagnostics for Combustion Temperature and Species (2nd ed.)* CRC Press, 1996. DOI: 10.1201/9781003077251.

[14] Wikimedia user: Vallastro. https://commons.wikimedia.org/wiki/File:Gaussian,_Lorentzian_and_Voigt_profiles.png. Accessed:2024-05-05.

[15] *Tunable Diode Laser Absorption Spectroscopy*. https://nanoplus.com/applications/tunable-diode-laser-absorption-spectroscopy. Accessed: 2024-05-31.

[16] Patrik Lundin. https://commons.wikimedia.org/wiki/File:GasmasPrinciple2.pdf. Accessed:2024-05-01.

[17] José Francisco Algorri et al. "Light Technology for Efficient and Effective Photodynamic Therapy: A Critical Review". In: *Cancers* 13.14 (2021). ISSN: 2072-6694. DOI: 10.3390/cancers13143484. URL: https://www.mdpi.com/2072-6694/13/14/3484.

[18] Ashleyj . Welch and M.J.C. van Gemert. *Optical-Thermal Response of Laser-Irradiated Tissue*. 1995. URL: https://api.semanticscholar.org/CorpusID:238627476.

[19] Romina Ronquillo. *Understanding Heat Exchangers*. https://www.thomasnet.com/articles/process-equipment/understanding-heat-exchangers/. 2022.

[20] Andrew C. Wilson et al. "Narrow-linewidth master-oscillator power amplifier based on a semiconductor tapered amplifier". In: *Appl. Opt.* 37.21 (1998), pp. 4871–4875. DOI: 10.1364/AO.37.004871. URL: https://opg.optica.org/ao/abstract.cfm?URI=ao-37-21-4871.

[21] Märta Lewander et al. "Nonintrusive gas monitoring in neonatal lungs using diode laser spectroscopy: feasibility study". In: *Journal of Biomedical Optics* 16 (12 2011), p. 127002. ISSN: 10833668. DOI: 10.1117/1.3663211.

[22] Y Ito et al. *Assessment of heating effects in skin during continuous wave near infrared spectroscopy*. 2000. DOI: 10.1117/1.1287730.

Appendix A

Data Analysis

Below the process of obtaining the different value demonstrated in the result section will be presented. Before showing the actual data analysis process however, the different signals have to be evaluated, while they are shown here, the explanation of the signals can be found in the method chapter.

A.1 Signals Obtained

The data that is obtained from the photo-diode is recorded by the oscilloscope in four different forms which will be described below. To simplify the communication the signals will from this point be described using letters instead A,B, C and D.

- **Unprocessed signal (A-signal):** This signal denotes one signal sweep that is transmitted from the photo-diode to the oscilloscope. While not representative of the entire series of measurements, it gives a qualitative representation of what might be instantaneously obtained in a clinical setting.
- **Time averaged signal (B-signal):** This signal is obtained by setting the oscilloscope to record an average of the A-signal over numerous sweeps. In this study, that average was over 300 signals being averaged over time. This improves the SNR of the signal considerably.
- **Moving average signal (C-signal):** This is the A-signal with a moving average filter applied to it during the data collection in the oscilloscope.
- **Averaged moving average signal (D-signal):** This signal is obtained by setting the oscilloscope to record an average of the C-signal over numerous sweeps. In this study, that average was over 300 signals being averaged over time. Similarly to the B-signal, this was shown to improve SNR.

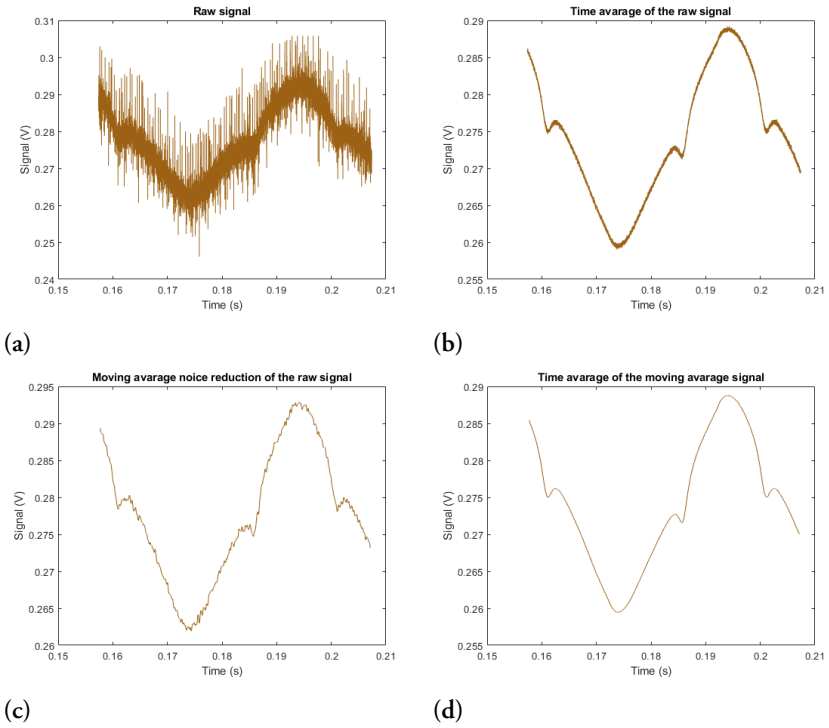

Figure A.1: The four different signals that are obtained from the oscilloscope when measuring. The unprocessed signal (a), the time average of the unprocessed signal (b), the moving average noise reduction of the unprocessed signal (c) and the time average of the moving average signal (d).

It is quite clear from observing the signals that the time average of the moving average signal (d) has the highest SNR while the unprocessed signal (a) has the lowest SNR. While the GASMAS signal is viable in the unprocessed signal, it is quite more visible for the other signals.

Moving forward these signals will be denoted as A-signal (unprocessed signal), B-signal (time average of the unprocessed signal), C-signal (Moving average noise reduction of the unprocessed signal) and D-signal (time average of the C-signal).

A.2 Absorption Fraction

The end goal of the signal processing is to find how much the signal is decreased as a result of the oxygen content in the tissue. This process includes many different steps that will be described below.

Isolating one Sweep

The first step is to isolate one of the sweeps that are present in the signal. To gain the full information of the signal, the center sweep with a positive tilt will be selected. This can be done either by cutting the signal from the lowest value to the highest value or by manually finding the indexes where cutting is appropriate. If the signal was perfect, it would be efficient to just pic the maximum and minimum values for isolating the signal. But since the peaks and valleys are not as sharp as is wished, it is more efficient to manually find the places where the signal becomes linear. While this may seem inefficient, the indexes of these positions will not change between the different signals which makes the process easily made into an algorithm. Since the time average of the moving average signal is the signal with the highest SNR, this is the one that will be used for the analysis. Below is a figure showing the appropriate values to isolate the signal for further processing as well as the cut signal.

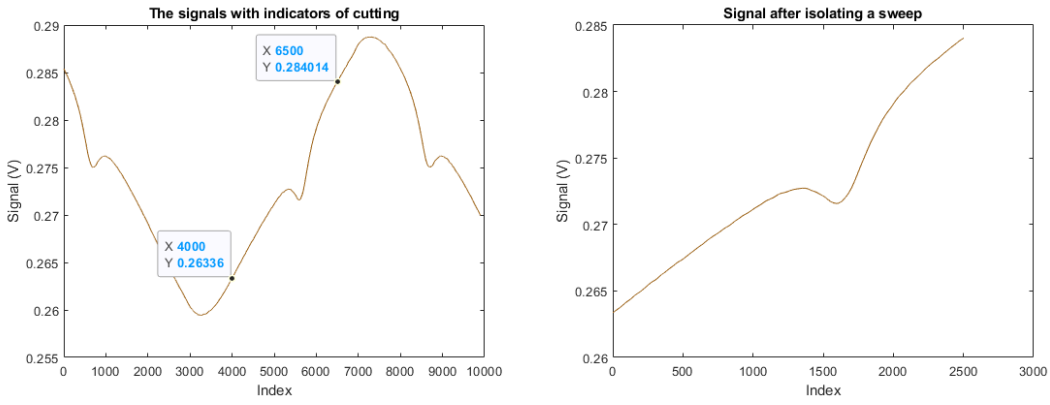

(a) (b)

Figure A.2: The process of determining where the signal is to be cut to isolate a sweep (a) as well as the resulting signal after being isolated (b).

Linear Regression

Since the intensity of the laser is increasing linearly the signal should be able to be fitted to a first order polynomial. This process will let us determine how the signal would look if the oxygen gas did not absorb some of the intensity. To achieve this, the actual decrease will have to be removed from the signal. Similarly to the isolation of a sweep, this will be done manually, but in the same way as for the sweep, the signal will fall on the same indexes for all measurements which automates the process. Below, the signal with the decrease removed can be seen along with the resulting linear regression together with the signal.

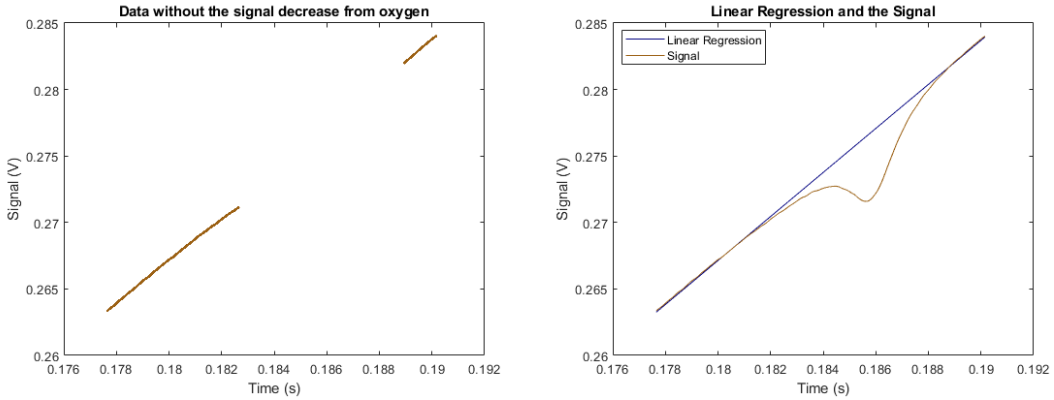

(a) (b)

Figure A.3: The signal after removing the decrease in signal (a) and the resulting linear regression along with the signal (b).

Finding the Fraction

From this stage to get the absorption, the position of the maximum decrease has to be found. This is most easily done by subtracting the linear regression from the signal and then finding the minimum value. This also isolates the shape of the absorption which will be used to evaluate broadening. Below this figure can be seen. From the values obtained at the biggest difference, the fraction of signal absorbed can easily be calculated.

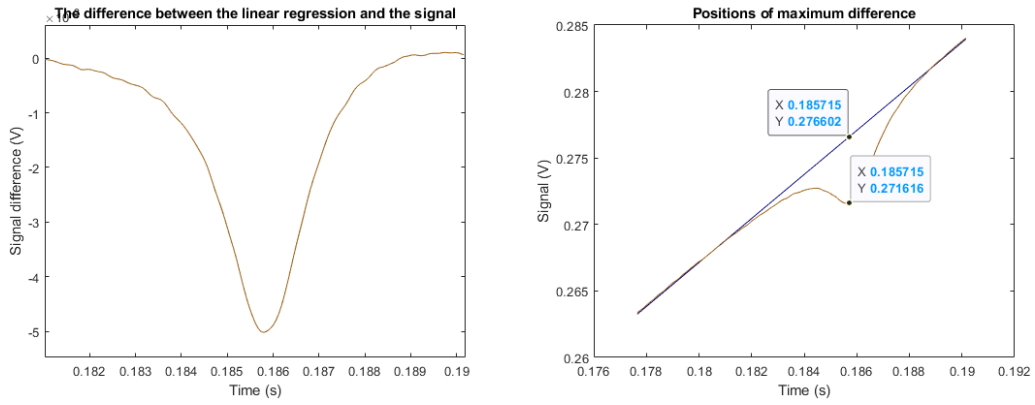

(a) (b)

Figure A.4: The isolated decrease in signal due to absorption by oxygen, the difference between the linear regression and the signal (a) and the points of maximum difference between the linear regression and the signal (b).

Nitrogen Adjustment

To ensure that the present signal comes from the oxygen content in the lungs, nitrogen was used in the same setup. The first step is to adjust the nitrogen signal. Due to slight adjustments in the measurements, the signals wont always align in strength. To combat this fact, the maximum and minimum points of the signals are compared and the nitrogen signal is aligned by creating a linear fit to these values. The adjustment is shown below.

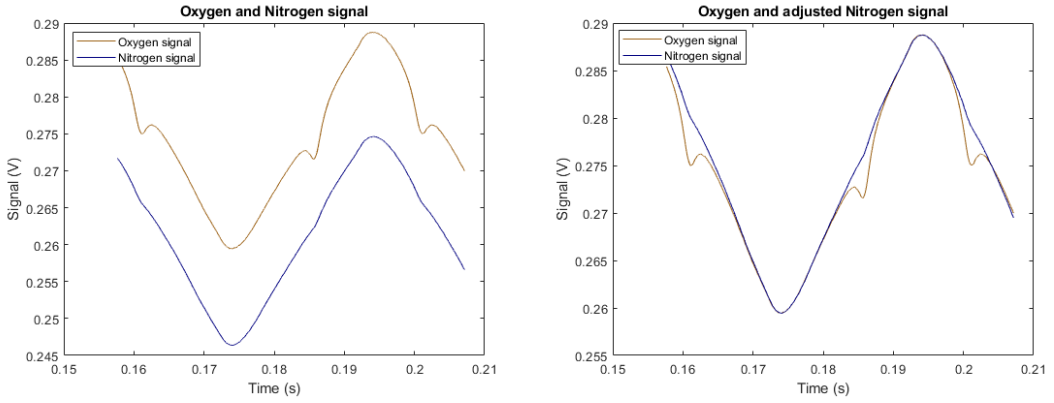

(a) (b)

Figure A.5: The oxygen and nitrogen signals (a) and the oxygen signal along with the adjusted nitrogen signal (b).

To adjust the absorption value the process is very similar to getting the initial absorption value. The only difference is that instead of the linear regression being used as the maximum value, the nitrogen signal is used.

A.3 Signal to Noise Ratio

The signal-to-noise ration is a parameter useful to determine if a signal is detectable or not. SNR comes in many different forms, for this thesis the signal will be the difference between the linear regression and the signal at the lowest depth. The more noisy signals will be time averaged to get the signal depth. The value

will be divided by the standard deviation of the signal. Below, the steps of this process will be shown. In the demonstration the unprocessed signal will be used.

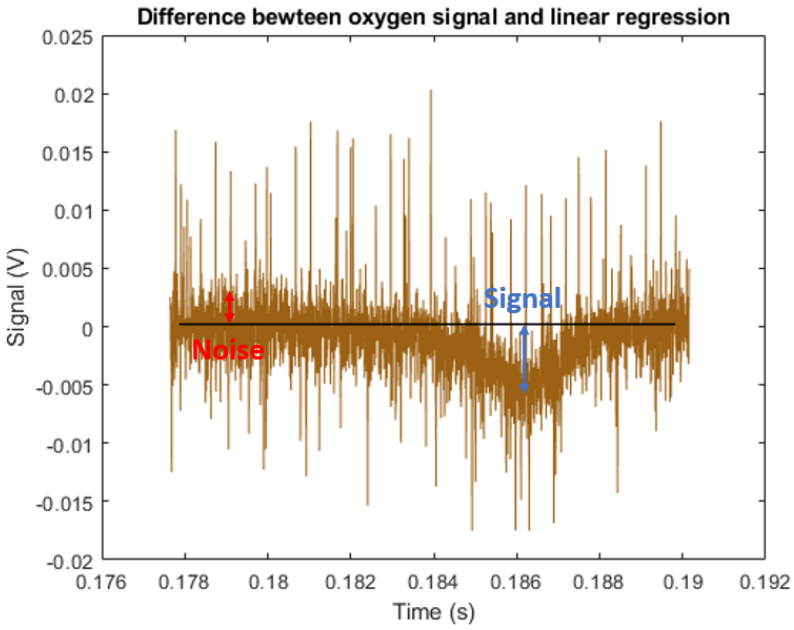

Figure A.6: The unprocessed signal (A-signal) showing which values will be used to calculate the SNR.

Smoothing the Signal

The first steps is the same as seen above to obtain the absorption. The difference between the linear regression and the signal will be used in obtaining the SNR. The signal is smoothed by a moving average to obtain the strength of the decrease. Below, the smoothing can be seen, a 100 point moving average is used. The minimum value of this smoothed difference will give the signal in SNR calculation.

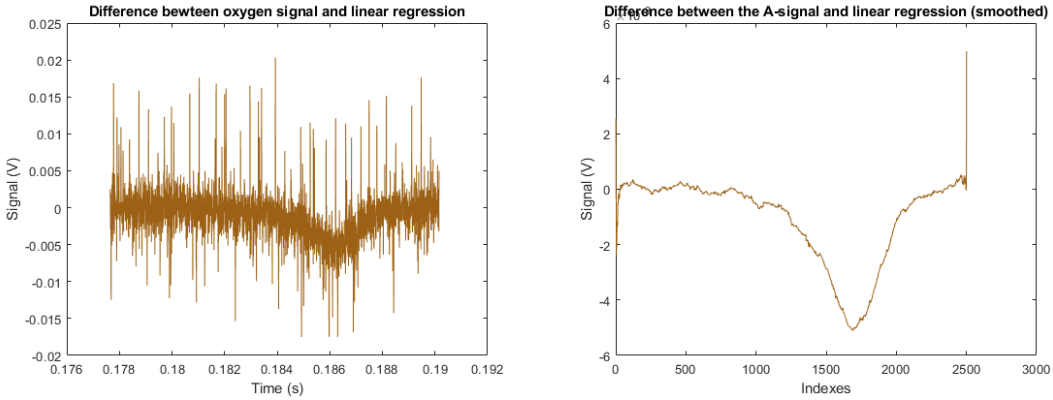

Figure A.7: The difference between the A-signal and the linear regression (a) and the smoothed version of the difference between the A-signal and the linear regression (b).

Obtaining the Noise

The noise is obtained by cutting out a section from the unsmoothed signal and calculating the standard deviation of the signal. Below, the noise plot is shown.

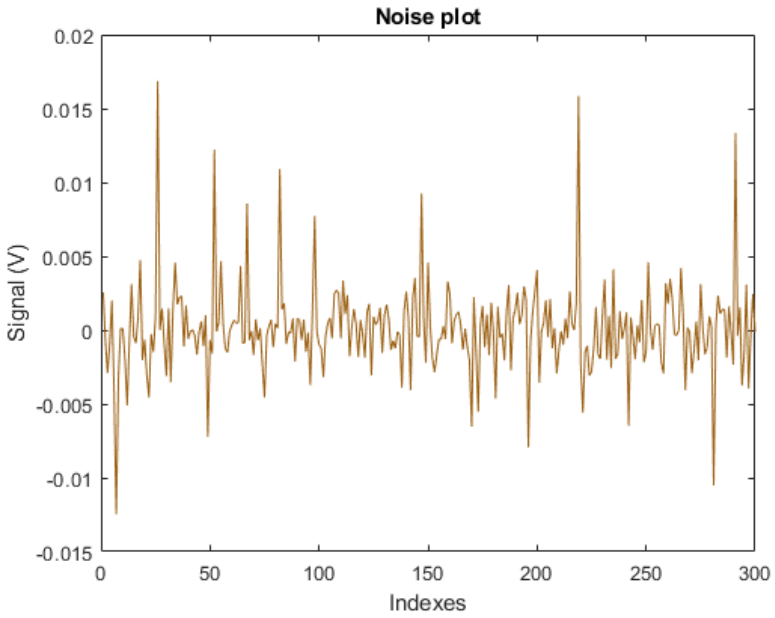

Figure A.8: A part of the difference between the linear regression and the A-signal used for noise calculation.

The SNR is then calculated by dividing the signal obtained from the smoothing by the standard deviation obtained from the noise. The resulting SNR in this case is calculated to be 1.8.

Appendix B

GASMAS Signals

Below, the figures for each of the measurements will be presented. While there are many different figures that are created in the process. A selection will be presented here.

- The unedited oxygen and nitrogen signals (D-signal).
- The oxygen signal along with the linear regression and nitrogen signal.
- The difference between the oxygen signal and the nitrogen signal.
- The difference between the oxygen signal and the linear regression.

2E12

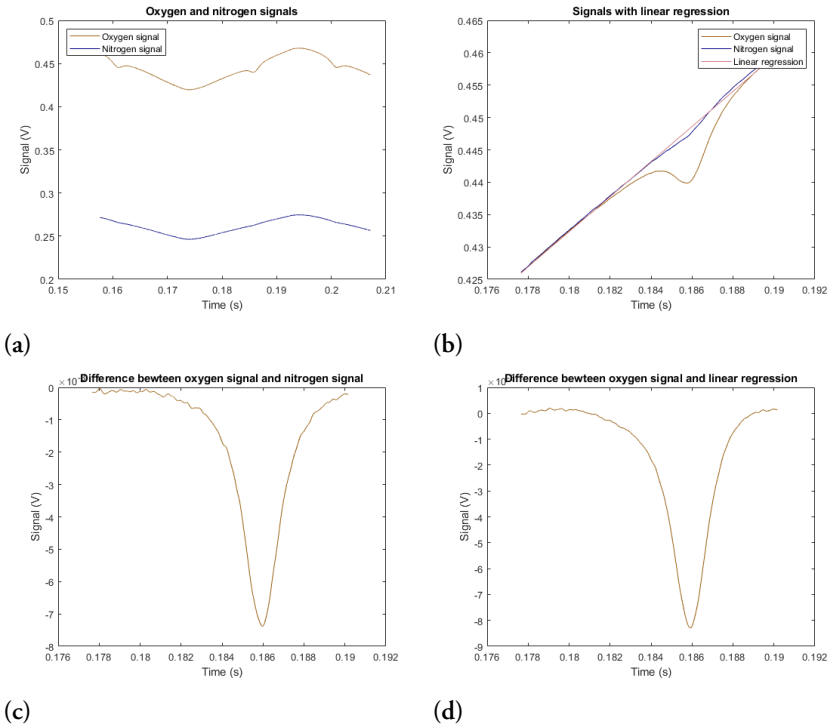

Figure B.1: The figures from measurement 2E10.

2E12

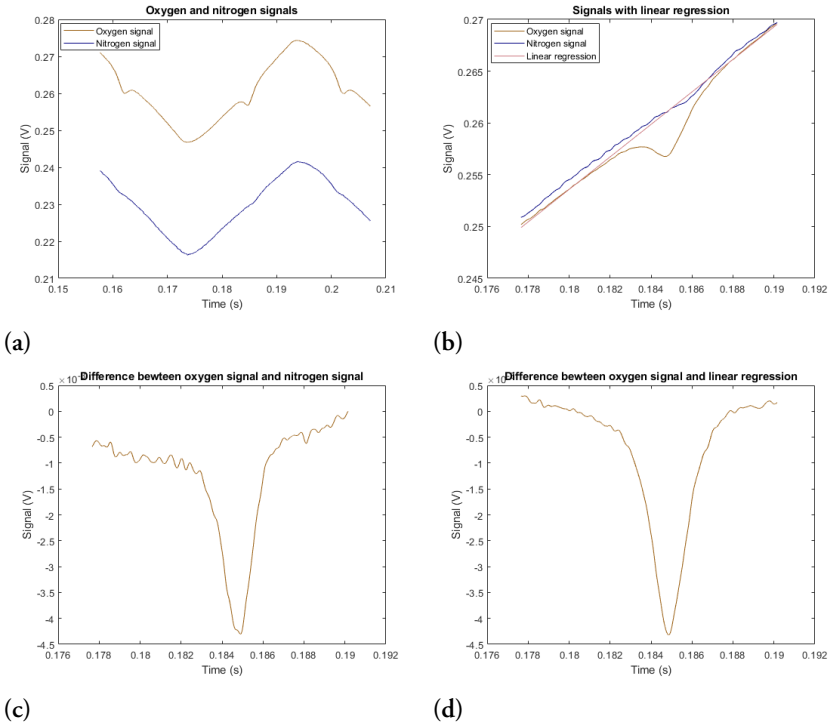

Figure B.2: The figures from measurement 2E12.

2E14

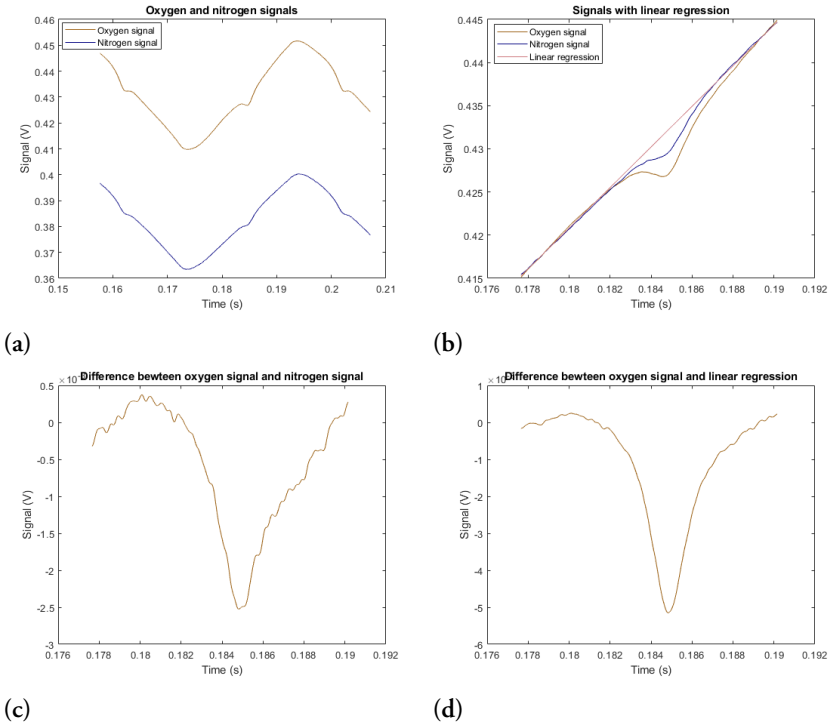

Figure B.3: The figures from measurement 2E14.

3I30

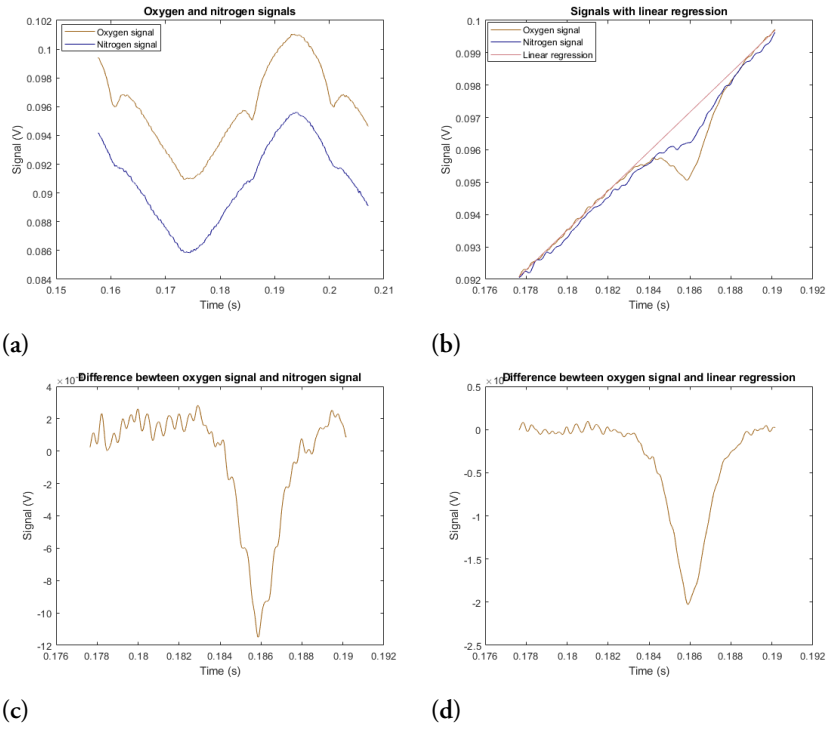

Figure B.4: The figures from measurement 3I30.

3I32

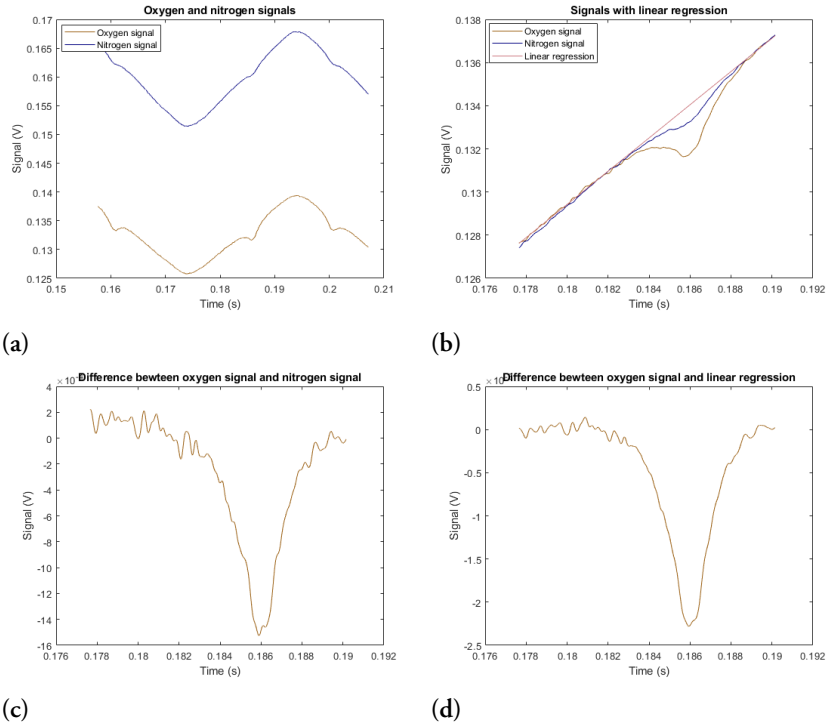

Figure B.5: The figures from measurement 3I32.

3I34

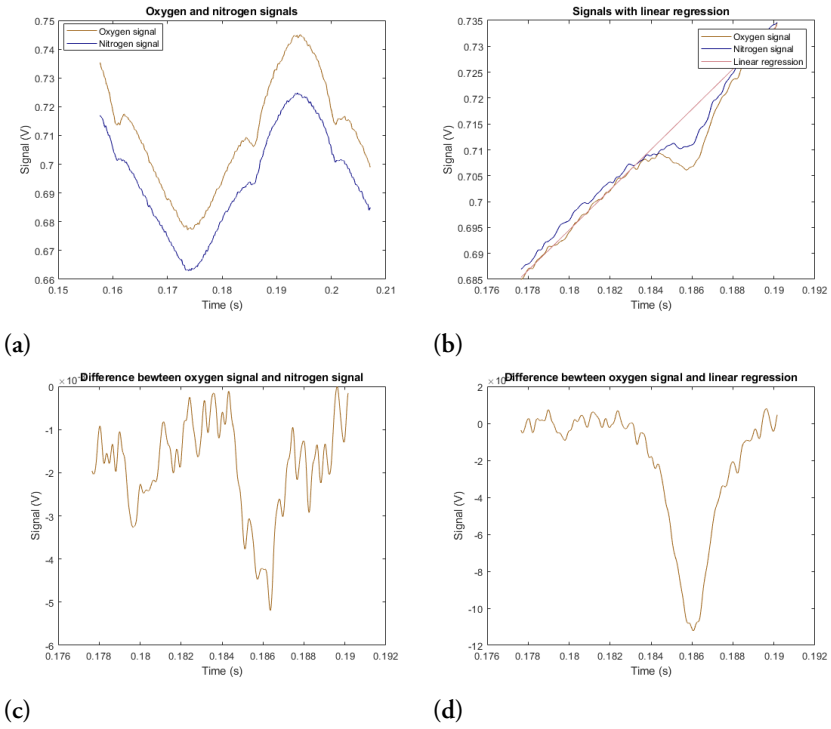

Figure B.6: The figures from measurement 3I34.

4E20

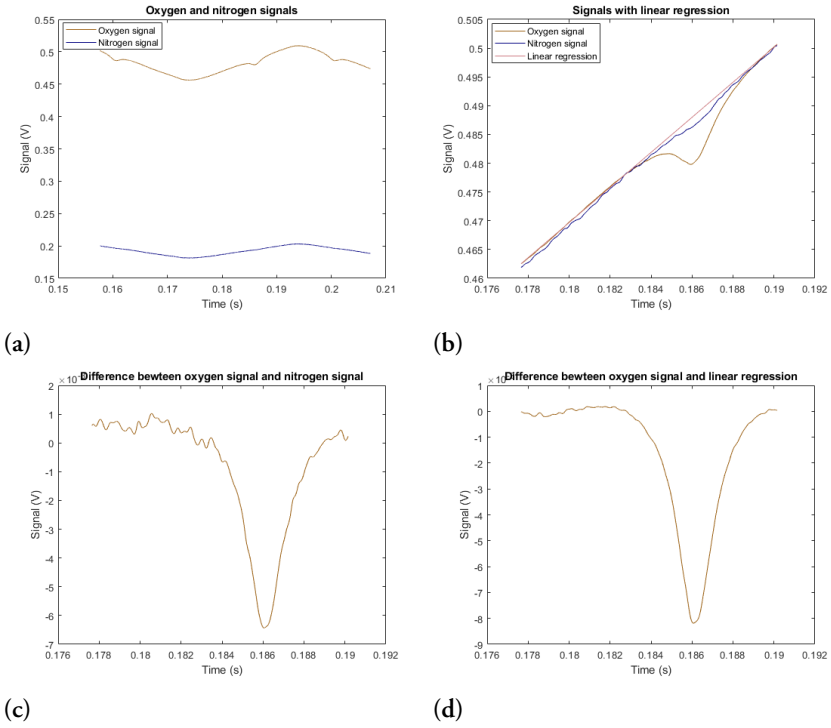

Figure B.7: The figures from measurement 4E20.